The impact of long-term operation on the Faradaic efficiency of Fe(0)-electrocoagulation

Universiteit Utrecht

Simon Müller 5657075

1st supervisor dr. Thilo Behrends
2nd supervisor dr. Case van Genuchten

August 31, 2017

Thesis submitted for the degree of Master of Science

Department of Earth Sciences
Faculty of Geosciences
Utrecht University

Abstract

Arsenic contamination of drinking water remains the largest chemical threat to millions of people, especially in rural Southeast Asia. One unconventional water treatment method that can be applied in remote communities is Iron-Electrocoagulation (Fe-EC), which is based on the electrochemical production of Fe-oxides in the contaminated water that bind arsenic. Although Fe-EC has been shown to effectively remove arsenic in extended field trials, the efficiency of field systems is several times lower than in laboratory studies and electrode surface layers are observed. We hypothesize that the Faradaic efficiency (*FE*) of field system is low, so that the generated Fe dose is lower than predicted by Faraday's law of electrolysis. However, no long-term systematic studies have been performed in the laboratory to evaluate the impact of long-term operation on the *FE*. We performed laboratory experiments investigating the long-term *FE* over a range of conditions for 15 – 35 runs. We tested different electrolytes, Fe(0) anode purity, and varied operation parameters like charge dosage rate and polarity alternation. Our results show that the *FE* does decline continuously during repeated operation under typical field conditions, resulting in a lower Fe dose than expected. In addition, we find that a high *FE* can be maintained in electrolytes free from oxyanions or by applying charge dosage rates ≥ 15 C/L/min. The results also suggest that a low *FE* is related to the formation of macroscopic surface layers on the electrodes. Based on these results, we discuss potential strategies to maintain the efficiency of Fe-EC field systems under realistic conditions and evaluate the implications for arsenic removal.

Acknowledgements

I would like to thank Case van Genuchten, who initiated and supervised my thesis project. I am especially grateful for his excellent support, positive feedback, and his infinite motivation. I thank Thilo Behrends, without whose support and supervision the project would not have been possible. A special thanks to Peter Kraal for his outstanding support both in the laboratory and in general. Also, I would like to thank Alwina Hoving and Helen King for the provided lab equipment and their helpful hints. Furthermore, I thank Thom Claessen, Coen Mulder, and John Visser for their assistance in the laboratory.

Abbreviations

If applicable with common synonyms and units.

CDR	Charge dosage rate	[C/L/min]
Fe-EC	Iron-electrocoagulation synonyms: Fe(0)-electrocoagulation	
FE	Faradaic efficiency synonyms: current efficiency, coulombic efficiency	[mass Fe/mass Fe]
IP	(Anode) interface potential synonyms: E_A	[V vs Ag/AgCl]
SGW	Synthetic groundwater	
SL	Surface layer synonyms: Oxidation layer, rust layer, oxide layer	

Contents

1. Introduction

Arsenic contamination of drinking water remains one of the largest chemical threats to decentralized populations in rural South-East Asia (Sharma et al. 2014). Arsenic (As) is naturally present in ground water aquifers worldwide (Nordstrom 2002), but the arsenic contamination is most severe around the Ganges-Brahmaputra delta in Bangladesh and West Bengal (India), where it affects millions of people (Nickson et al. 1998). The long-term intake of drinking water with elevated As concentrations can cause different types of cancer and skin lesions (Flanagan et al. 2012). Argos et al. (2010) estimated that 20% of all adult deaths in Bangladesh can be attributed to arsenic exposure > 10 µg/L in drinking water, a major public health crisis (arsenic crisis). When arsenic-free water sources, for example surface water, are not available or increase the risk of water-related infectious disease, treatment of As contaminated ground water is the only option (Lokuge et al. 2004).

Conventional methods for arsenic removal (e.g. adsorbents (Mohan and Pittman 2007) or chemical coagulants (Hering et al. 1997)) are inadequate to solve the arsenic crisis, which primarily affects rural populations in low-income regions without reliable drinking water infrastructure. A promising alternative treatment method is Iron-Electrocoagulation (Fe-EC), which is based on the addition of coagulants produced in situ by electrochemical oxidation of a sacrificial metal anode. Fe-EC can remove a range of contaminants (e.g. (heavy) metals (Akbal and Camcı 2011, Yang et al. 2015), dyes (Aleboyeh et al. 2008), oil (Chen et al. 2000), E. coli (Delaire et al. 2015)) from different source waters, but Fe-EC is especially suitable for low-cost As removal in decentralized rural communities. The EC reactor can be manufactured with locally available materials (Amrose et al. 2014). The operating costs, steel and electric energy consumption, are low and the system can be operated by local staff (Amrose et al. 2014). In comparison to chemical coagulation, no storage and dosing of chemicals is required. Unlike conventional sorption techniques, pre-oxidation of As(III), which has a much lower sorption affinity than As(V), is not necessary (Hug and Leupin 2003). Field trials with a 600 L batch reactor in West Bengal (India) showed the ability of Fe-EC to consistently remove As below 5 µg/L from local groundwater for several months (Amrose et al. 2014), meeting the maximum concentration for drinking water recommended by the WHO (2017) of 10 µg/L.

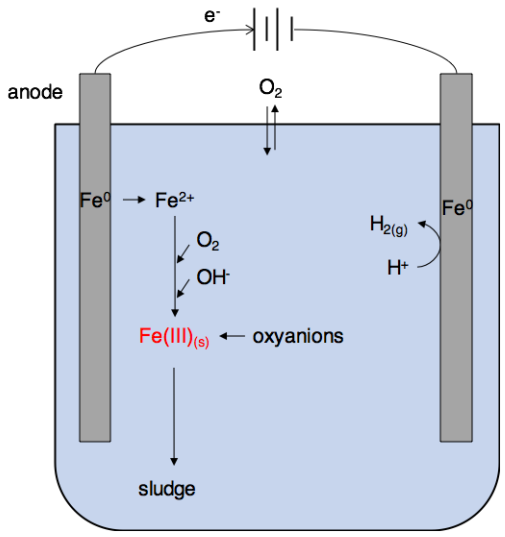

Figure 1. Principle of Fe-electrocoagulation

While the Fe-EC setup and operation is simple, the underlying (electro-)chemical reactions are more complex (Figure 1). In Fe-EC, a direct current is applied to oxidize the Fe(0)-anode to generate Fe(II) in solution (Lakshmanan et al. 2009):

$$Fe^0 \rightarrow Fe^{2+} + 2\,e^- \quad (1)$$

For As removal with Fe-EC, the produced Fe(II) in the bulk electrolyte is oxidized by dissolved oxygen to generate Fe(III) precipitates (van Genuchten et al. 2014). Dissolved As(V) forms surface complexes on these Fe precipitates (van Genuchten et al. 2012) and arsenic can be removed subsequently by gravitational settling or filtration of the solids. Simultaneously, As(III) is oxidized to As(V) by reactive intermediates that form during the oxidation of Fe(II) (Li et al. 2012), which makes Fe-EC effective for As removal independent of its oxidation state. On the cathode, hydrogen gas is produced (Lakshmanan et al. 2009):

$$2\,H^+ + 2\,e^- \rightarrow H_{2(g)} \quad (2)$$

In all applications of Fe-EC, the applied current I is a key operating parameter because it is proportional to the Fe(II) production rate. In addition, several other variables are essential to describe the Fe-EC system sufficiently: the anode surface area A_A, the electrolyte volume V, and the electrolysis time t for which the current is applied. Operating parameters derived from these variables are typically used in EC literature, like the current density i (mA/cm^2, Eq. 4), the charge dosage rate CDR (C/L/min, Eq. 5), and the total charge dose q (C/L, Eq. 6).

Table 1. Operating parameters for Electrocoagulation systems and typical units derived from the applied current I (A), the anode surface area A_A (cm^2), the electrolyte volume V (L), and the electrolysis time t (s).

Current density	$i = \frac{I}{A_A}$	(4)	mA/cm^2
Charge dosage rate	$CDR = \frac{I}{V} = i * \frac{A_A}{V}$	(5)	C/L/min
Total charge dose charge density	$q = \frac{I * t}{V}$	(6)	C/L
Faradaic efficiency current efficiency, coulomb efficiency	$FE = \frac{[Fe]_{measured}}{[Fe]_{faraday}}$	(7)	% or no unit
Iron dose	$[Fe] = FE * \frac{I * t * M}{n * F * V}$	(8)	mg/L

Despite advances in Fe-EC research in recent years – lab and field studies showed its effectiveness for As removal under various conditions – long-term operation in the field revealed a number of issues: The arsenic removal efficiency (the mass of As removed per charge passed for final [As] < 10 µg/L) of the Fe-EC system tested in West Bengal is up to five times lower than the efficiency of systems tested in the laboratory (Amrose et al. 2014, van Genuchten et al. 2016). Several parameters can contribute to this decrease in performance under field conditions. For example, changes in electrolyte composition, either the presence of competing oxyanions or reduced species, can decrease As removal efficiency (Pallier et al. 2011, Roberts et al. 2004). In addition, the operating parameters, a high CDR, and corresponding low O_2 saturation negatively affect As(III) removal (Delaire et al. 2017). During the field trials, a further decrease in removal efficiency and an increase in cell voltage could be counteracted by lightly brushing the electrode surface (Amrose et al. 2014).

A possible explanation for these changes over time is that Fe concentrations in the bulk electrolyte have decreased. Assuming that the oxidation of Fe(0) to Fe(II) is the only reaction on the anode, one can use Faraday's law (Eq. 3) to calculate the amount of Fe generated during Fe-EC.

$$[Fe]_{faraday} = \frac{I * t}{n * F * V} \quad (3)$$

With n = 2 for Fe(II) and Faraday's constant F = 96485 C/mol

This assumption has been confirmed in controlled laboratory studies (e.g. Lakshmanan et al. (2009), Mansouri et al. (2011)). However, extended field trials of EC field units for seawater pretreatment showed that Faraday's law does not accurately predict Fe concentrations in the bulk electrolyte (Timmes et al. 2010) and studies investigating Fe production over time rather than specific removal efficiencies are rare.

To examine if Fe production in the Fe-EC system is inefficient, we can use the Faradaic efficiency (*FE*, also called current efficiency, coulomb efficiency, or charge yield in the EC literature (Chen et al. 2000, Mechelhoff et al. 2013, Sillanpää and Shestakova 2017, Timmes et al. 2009)). The *FE* is defined as the measured Fe concentration in the bulk electrolyte normalized by the Fe concentration predicted by Faraday's law (Equation 3 & 7). A *FE* of 1 means ideal Fe production on the anode as predicted by Faraday's law. That is, all charge passed through goes to Fe(II) production and transport to the bulk electrolyte. A *FE* < 1 suggests that Fe production and transport to the bulk is not ideal, resulting in a lower Fe dose (Eq. 8). A low *FE* can originate from two main reasons, (a) Fe(0) oxidation is limited or absent due to competing side reactions (e.g. oxidation of water) or (b) Fe(II) is produced but does not end up in the bulk electrolyte.

Competing oxidation reactions are favored at the anode-water interface at high anodic interface potentials (*IP*), which can occur when high current densities are applied (Dubrawski et al. 2015). High *IP* can also originate from the formation of an anodic passive layer – a nanometer thick, invisible, and nonporous layer that inhibits the transfer of ions between anode surface and electrolyte (Cornell and Schwertmann 2003, Schultze and Lohrengel 2000). While passive layers that limit corrosion are desired on steel used for most applications, the formation of passive layers in the EC system must be prevented since Fe(0) oxidation is the key process. The electrolyte composition is essential for the (de-)passivation of iron. Phosphate or nitrate in single oxyanion electrolytes led to low *FE,* likely due to passivation, whereas chloride and bromide electrolytes resulted in a high *FE* (van Genuchten et al. 2017). Furthermore, chloride, known to promote steel corrosion (Cornell and Schwertmann 2003, Frankel 1998), may also maintain high *FE* in oxyanion-rich electrolytes (van Genuchten et al. 2017).

Although (nanoscale) passive layers have the potential to decrease the *FE* of Fe-EC systems, actual field trials observed the formation of macroscopic layers on the electrode surfaces. In contrast to passive layers, we define macroscopic modifications of the anode or cathode surfaces as surface layer (SL). Passivation might occur underneath a surface layer, but the term passivation is also used to describe porous iron oxide or carbonate deposits on electrodes, which makes it ambiguous. A low *FE* could occur if Fe(0) is oxidized but subsequently deposited on the electrodes

(SL formation) or trapped by existing surface layers, independent of electrode passivation, and this process is likely to be time dependent.

The formation of surface layers is often stated as a disadvantage of EC (Mollah et al. 2001), but only a few studies have investigated long-term (Faradaic) efficiency and possible interactions. Lakshmanan et al. (2009) observed anode surface rusting and a decrease in *FE* over a time of 15 days in a laboratory Fe-EC study. Mechanical cleaning of the anode was applied and led to a constant Fe generation at high *FE*. In fact, most EC studies mention the potential problems associated with surface layers and avoid it by mechanical or acid cleaning of the electrode surfaces before each experiment to ensure reproducibility (e.g. Pan et al. (2016), Dubrawski et al. (2015)). Timmes et al. (2010) observed the formation of surface layers, characterized as a mixture of Fe(III) and Fe(II/III) minerals, and identified low flow velocities as a potential reason. The surface layers of the EC system in West Bengal were found by van Genuchten et al. (2016) to consist mainly of magnetite. The observed decrease in performance was attributed to the formation of these layers, trapping Fe(II) produced on the anode surface (van Genuchten et al. 2016). In addition to electrode cleaning, reversing the polarity between the electrodes is recommended to avoid surface layer formation or passivation. The ideal time interval, however, is unclear and, as a consequence, polarities are reversed at time intervals between days and less than a second (Amrose et al. 2014, Mansoorian et al. 2014, Xie et al. 2017, Yang et al. 2015). A consistent result is a lower electricity consumption, but the effect on the *FE* and long-term effects in general remain unclear.

Based on the field trials by Amrose et al. (2014) and the available literature, we expect that the *FE* of Fe-EC systems decreases as the number of runs, which includes wet (operation) and dry (storage) conditions, increases. We expect the decrease in *FE* is accompanied by an increase in the anodic *IP* and total cell voltage. In addition, the growth of an anodic surface layer is expected.

In this study, we track the *FE* of Fe-EC systems over long-term operation (15 – 35 runs) in the laboratory. Experiments are conducted to replicate typical conditions of the field Fe-EC system (Amrose et al. 2014) using synthetic groundwater, a low *CDR*, and steel anodes of low and high purity. After each run (between 8 – 105 min electrolysis time), electrodes are stored open to the atmosphere and the electrodes were left untouched. To identify the key (electro)chemical parameters that control the *FE* over long-term operation, we examined the impact of electrolyte composition and electrode material. In addition, we varied the applied current (*CDR* from 4 – 54 C/L/min), and investigate the effect of polarity reversal. The formation of macroscopic surface layers was documented and the solids were characterized by powder XRD. The results of this study help identify the parameters that govern the *FE* under realistic operating conditions. Based on our results, we propose options to maintain a high *FE* that can be implemented by operators of Fe-EC systems in the field.

2. Methods

2.1 Materials

All chemicals except for the anhydrous calcium chloride (≥ 90%, Merck) were reagent grade or higher. Solutions were prepared using ultrapure DI water. Glassware and PTFE coated stir bars were rinsed with hydrochloric acid and washed three times with DI water before each experiment. Oxygen concentrations and solution pH were measured with a Hach HQ40D (Hach LDO101 and PHC101 probes) or with an ORION VersaStar Pro multi-channel meter (ROSS Ultra pH/ATC Triode and ORION Star RDO optical probe). The conductivity was measured with a Hach CDC401 probe.

2.2 Electrolytes

The synthetic groundwater (SGW) electrolyte was prepared to represent the average groundwater in Bangladesh based on data from the British Geological Survey (BGS and DPHE 2001, Roberts et al. 2004). The concentrations of each electrolyte are given in Table 2. Batches of SGW were prepared by adding volumes of stock solutions of 0.8 M $NaHCO_3$ (Merck), 0.3 M $CaCl_2$ (Merck), and 0.2 M $MgCl_2 \cdot 6H_2O$ (Merck) to DI water. The pH of the solution was lowered below 7 by bubbling $CO_{2(g)}$. Under vigorous stirring, silicate was added from a freshly prepared alkaline 0.02 M stock solution ($Na_2SiO_3 \cdot 9H_2O$, Sigma-Aldrich). After the addition of the 0.1 M phosphate stock ($Na_2HPO_4 \cdot 7H_2O$, Sigma-Aldrich), the final pH and conductivity were measured. Due to its trace concentration, As was not added to the SGW used for long-term experiments. The SGW electrolyte was prepared in 10 L batches and stored in an air tight container.

To examine systematic variations of SGW composition, 2 L batches of modified SGW were prepared by excluding Ca and Mg for Soft-SGW and excluding carbonate, silicate, and phosphate for Oxyanion-free-SGW. Sodium chloride (Merck) was added to Soft-SGW to ensure equal chloride concentrations in all SGW variations (Table 2). We also examined electrolytes consisting of only 10 mM NaCl (1 L batches). For As removal experiments, arsenic contaminated groundwater was prepared in 1 L batches following the SGW recipe, with subsequent addition of As(III) from a fresh stock solution ($NaAsO_2$, Sigma-Aldrich) after phosphate addition.

Table 2. Electrolyte compositions in mM and measured conductivity in μS/cm.

	Na^+	Ca^{2+}	Mg^{2+}	HCO_3^-	Cl^-	HPO_4^{2-}	SiO_3^{2-}	As(III)	Cond.
SGW	10.4	2.5	2.5	8.2	8.2	0.1	1	0	1673
Soft-SGW	18.6	0	0	8.2	8.2	0.1	1	0	1752
Oxyanion-free-SGW	0	2.5	2.5	0	8.2	0	0	0	900
As-SGW	10.4	2.5	2.5	8.2	8.2	0.1	1	0.008	1686
NaCl	10	0	0	0	10	0	0	0	NA

2.3 Electrocoagulation experiments

The lab experiments were designed to reproduce the operating parameters of a 600 L batch reactor installed in a rural community in Dhapdhapi, West Bengal, India (Amrose et al. 2014). The reactor consisted of three 750 L tanks, one for electrolysis and two for settling. In the electrolysis tank, four electrode assembly cores were used, each with 10 parallel steel electrodes (625 x 250 x 4 mm). This reactor design results in an anode surface are of 6.25 m^2 and an electrode area to electrolyte volume ratio of approx. 100 cm^2/L. Alternate plates (2 cm distance) were electrically connected to a potentiostatic power supply and the polarity of the electrodes was reversed for each experiment. During electrolysis, the electrolyte was mixed with a turnover rate of approximately 3.5 reactor volumes per hour using a small electric pump.

This reactor was operated for months to treat arsenic contaminated local groundwater (266 ± 42 μg/L As). A current of 45 A was applied for an average treatment time of 105 min, equivalent to a charge dosage rate (*CDR*) of 4.3 C/L/min, a total dose of 450 C/L, and a current density of 0.7 mA/cm^2. These operating parameters were used in all experiments, unless otherwise noted. During electrolysis, the cell voltage was typically 2 – 4 V. The system was operated on most weekdays for 1 – 2 batches by a local operator. The batch system consistently reduced arsenic concentrations to below 5 μg/L, meeting the international standards for arsenic and iron in drinking water (WHO 2017).

2.3.1 Experimental procedure

The EC cell typically consisted of two steel electrodes (99% Fe, trace amounts of Mn and Cr) spaced 1 cm apart with a submerged anode surface area of 18 cm^2. Before the first run, the electrodes were cleaned with concentrated hydrochloric acid, rinsed with DI water, and polished with fine grained sandpaper. Experiments were conducted open to the atmosphere at 20 °C. An electrolyte volume of 200 mL was measured with a glass volumetric flask and transferred to a 200 mL glass beaker. The oxygen concentration of the electrolyte was decreased to 2.8 – 3.7 mg/L by bubbling N_2 gas and the pH was adjusted to pH 7 (± 0.1) by subsequent bubbling with CO_2. The solution was stirred with a PTFE coated stir bar. The speed was adjusted to ensure complete mixing, while avoiding turbulent mixing with vortex formation to best reproduce the laminar mixing in the field system. The electrodes were submerged and a constant current was applied using a bench top power supply (TENMA 72-10500) to achieve a *CDR* of 4 C/L/min. The current was measured before and after the experiment with a multimeter to account for small current drifts (typically < 1% of the applied current). The total cell voltage was measured throughout the reaction and logged after 20 min and just before the end of the experiment. The anodic interface potential was measured with a Ag-AgCl reference electrode (double junction, 3 M KCl) attached to a multimeter after 40 and 85 min. The reference electrode was placed just below the electrolyte surface and always at the side of the anode facing the bulk electrolyte, rather than in between the electrodes. The experiment was stopped after approximately 105 min and the actual treatment time was recorded. The electrodes were then carefully removed and stored on a rack open to the atmosphere at room temperature overnight (or in some cases, over the weekend). Electrolyte samples for the analysis of total Fe were taken with a wide mouth pipette after removing the steel electrodes but before the stirring was

stopped. The oxygen concentration and the pH were measured after each experiment. Each experiment was typically performed once each work day and the polarity was not reversed between each experiment, unless otherwise noted.

2.3.2 Summary of experimental conditions

A number of key electrochemical and solution parameters – i.e. the *CDR*, the anode material, and the electrolyte composition – were varied in separate experiments to evaluate the importance of these parameters on the Faradaic efficiency over time. In this section, we summarize the differences between each experiment. The major variables of each experiment are also given in Table 3 and a schematic is presented in Annex Figure 1.

Two experiments (Lab_04a and b) were performed in duplicate and used as a reference to compare all other experimental conditions. These reference experiments were performed as described in the previous section using steel electrodes at a charge dosage rate of 4 C/L/min in a SGW electrolyte over in total 41 runs (total time including storage 2.5 months). A set of seven experiments was used to investigate the effects of the anode material and the charge dosage rate on the Faradaic efficiency in SGW (Annex Figure 1A). For simplicity, we identify experiments using high purity Fe anodes with the prefix **Lab**, the experiments with an impure steel anode obtained directly from the field system installed in West Bengal, India (only 92% Fe and >1.5% Mn; (van Genuchten et al. 2016)) as **Field**, and experiments with aluminum electrodes as **Al**. The same anode surface area to volume ratio (A_A/V = 90 cm^2/L) was maintained in all experiments by reducing the electrolyte volume of experiments with the field anode (A_A = 9 cm^2) to 100 mL. The three materials were tested at a range of charge dosage rate from 4 C/L/min (equivalent to the field system) to above 50 C/L/min, which we identify by the suffix (i.e. Field_04 corresponds to the field anode operated at 4 C/L/min in SGW). All additional experiments described below were conducted with laboratory electrodes, which is not explicitly stated in their short names.

In the next set of experiments, we evaluated the impact of electrolyte chemistry (Annex Figure 1B) on the Faradaic efficiency over time. Sodium chloride (10 mM) was used as an electrolyte with both low and high *CDR* (NaCl_04 and NaCl_54). Two modified SGW electrolytes were used to investigate the effects of oxyanions and Ca/Mg separately (Oxyanion-free; Soft-SGW) at *CDR* of 4 C/L/min.

Finally, we tested a number of potential options to improve the Faradaic efficiency (Annex Figure 1C). Alternating the polarity of the electrodes between each run, which is also done for the field system, was tested in experiment Polarity-1. In addition to polarity changes between runs, the polarity was alternated every 21 min during the electrolysis of experiment Polarity-5. Additional aeration was tested in experiment O2_54 to investigate the effect of higher O_2 concentrations on the *FE* at a high *CDR*, in contrast to all other experiments at a *CDR* above 4 C/L/min where O_2 was depleted at the end of electrolysis. The impact of water saturated electrode storage conditions was investigated in experiment SGW-Storage by submerging the electrodes in SGW immediately after electrolysis

Table 3. Summary of experiments and their average operating parameters. The numbers represent the average and one standard deviation of replicate experiments. The anode surface area was 18 cm^2 except for experiments with the field anode (A_{Field} = 9 cm^2) and the same anode surface area to volume ratio (A/V = 90 cm^2/L) was maintained in all experiments.

Experiment	Anode current density	Charge dosage rate	Coulombic dose	No. of runs	Treatment time	Electrolyte	Anode Material	Initial pH	Final [O_2]
	mA/cm²	*C/L/min*	*C/L*		*minutes*				*mg/L*
Lab_04a	0.80 ± 0.00	4.34 ± 0.01	456 ± 2	41	105.1 ± 0.1	SGW	Fe lab	7.0 ± 0.1	3.7 ± 1.1
Lab_04b	0.80 ± 0.03	4.29 ± 0.14	451 ± 15	20	105.0 ± 0.2	SGW	Fe lab	7.0 ± 0.0	3.9 ± 0.9
Lab_15	2.8 ± 0.0	15.0 ± 0.0	451 ± 2	15	30.1 ± 0.1	SGW	Fe lab	7.0 ± 0.1	0.1 ± 0.1
Lab_32	6.0 ± 0.0	32.3 ± 0.0	453 ± 1	15	14.0 ± 0.0	SGW	Fe lab	7.0 ± 0.1	0.2 ± 0.1
Lab_54	10.0 ± 0.0	54.0 ± 0.1	451 ± 5	20	8.4 ± 0.1	SGW	Fe lab	7.0 ± 0.1	0.2 ± 0.1
Field_04	0.80 ± 0.01	4.29 ± 0.03	451 ± 3	20	105.0 ± 0.0	SGW	Fe field	7.0 ± 0.0	3.0 ± 0.9
Field_54	10.2 ± 0.0	54.9 ± 0.0	461 ± 7	15	8.4 ± 0.1	SGW	Fe field	7.2 ± 0.5	0.2 ± 0.1
Al_04	0.78 ± 0.01	4.23 ± 0.03	445 ± 3	15	105.0 ± 0.1	SGW	Al	7.0 ± 0.1	5.0 ± 0.5
Al_54	10.0 ± 0.0	54.0 ± 0.0	450 ± 2	15	8.3 ± 0.0	SGW	Al	7.0 ± 0.1	2.8 ± 0.8
Soft-SGW	0.78 ± 0.00	4.19 ± 0.01	440 ± 2	15	105.1 ± 0.3	Soft-SGW	Fe lab	7.0 ± 0.1	3.4 ± 0.9
Oxyanion-free	0.81 ± 0.00	4.35 ± 0.01	457 ± 1	15	105.1 ± 0.1	Oxyanion-free	Fe lab	6.8 ± 0.5	3.3 ± 0.6
NaCl_04	0.81 ± 0.00	4.37 ± 0.01	459 ± 1	20	105.1 ± 0.1	NaCl	Fe lab	8.8 ± 0.7	2.3 ± 0.8
NaCl_54	10.0 ± 0.0	53.9 ± 0.0	450 ± 1	20	8.3 ± 0.0	NaCl	Fe lab	8.5 ± 0.8	0.2 ± 0.1
O_2_54	10.0 ± 0.0	53.9 ± 0.0	450 ± 3	15	8.3 ± 0.0	SGW	Fe lab	7.0 ± 0.1	6.0 ± 0.7
Polarity-1	0.81 ± 0.01	4.37 ± 0.04	459 ± 4	15	105.0 ± 0.0	SGW	Fe lab	7.0 ± 0.1	3.7 ± 0.8
Polarity-5	0.77 ± 0.00	4.18 ± 0.01	439 ± 1	20	105.0 ± 0.0	SGW	Fe lab	7.0 ± 0.1	4.6 ± 0.5
SGW-storage	0.81 ± 0.00	4.39 ± 0.03	461 ± 3	20	105.1 ± 0.1	SGW	Fe lab	7.0 ± 0.0	4.3 ± 0.8

2.4 Wet chemical analysis

A modified (APHA 2005) protocol was used for measurements of total Fe in the bulk electrolyte. The samples containing iron precipitates were dissolved and reduced to Fe^{2+} in a solution containing concentrated HCl (32%, Merck) and excess hydroxylamine (Merck). After complete dissolution, the pH was adjusted to 3.3 with ammonium acetate (Merck) and 1,10-phenanthroline (Sigma-Aldrich) was added, forming an orange-red complex with Fe^{2+}. The absorbance of the samples was measured at 510 nm (Shimadzu UVmini-1240).

Arsenic samples and aluminum samples were acidified with 5% HNO_3 (Merck) and measured by atomic absorption spectrometry (AAS) using an AAnalyst 800. The arsenic measurements were performed in graphite furnace mode, whereas the aluminum measurements were performed in flame mode.

2.5 Quantification and characterization of surface layers

Surface layers formed on the anodes and cathodes were quantified by two methods.
The first method entailed cutting a small section (4 x 20 x 1 mm) from the bottom of the electrodes and submerging the electrode sections in nitric acid to remove the oxidized iron corrosion layer. Concentrated nitric acid (69%, Merck) was selected to minimize the dissolution of Fe(0) (Kelly et al. 2002), which was confirmed in control experiments that showed no dissolution of clean Fe(0) electrodes upon exposure to the nitric acid. After submerging the electrode pieces for 12 hours, they were removed from the nitric acid and washed with DI water. As solids remained in the solution, the extraction solution was diluted with concentrated HCl (Merck) to dissolve the remaining particles. After complete dissolution, samples were diluted with DI water and the concentrations of total Fe were measured colourimetrically.

The second method to quantify the amount of surface layer formed on the anodes and cathodes consisted of mechanically removing the surface layers with a brass brush and weighing the removed solids. The surface layer mass was normalized by the surface area of each electrode to obtain comparable numbers. The solids generated in these experiments were also ground with a mortar and pestle and analyzed by X-ray diffraction using a Bruker D-8 diffractometer with Cu K-alpha radiation and a rotating sample stage. Measurements were performed from 15 to 75° 2θ with 0.01° step sizes and total data collection times of approximately 4 h per sample. The absence of metallic Fe was confirmed by the XRD data, which confirms the reliability of the brushing method to remove only oxidized Fe layers.

Both quantification methods do also have drawbacks. The first method (HNO_3) does overestimate the amount of Fe per area of electrode if the SL is not homogenous in thickness or Fe content. The second method (brushing) does not completely remove very robust surface layers. However, other methods to remove these layer (e.g. sandpaper, steel brush) were not applied to avoid sample contamination with Fe(0) for subsequent XRD analysis.

2.6 Arsenic removal

For two experiments, Lab_04b and Field_04, SGW containing > 600 µg/L As(III) was used during run number 20 to assess the arsenic removal efficiency. Samples were taken during

electrolysis, at the end of electrolysis, and after one additional hour of mixing and directly passed through 0.2 μm filters. The surface layers were then mechanically removed for further analysis and the electrodes were cleaned with concentrated HCl and fine-grained sandpaper. The arsenic removal experiments were then repeated with the cleaned electrodes to determine the impact – if any – of the electrode surface layers on arsenic removal.

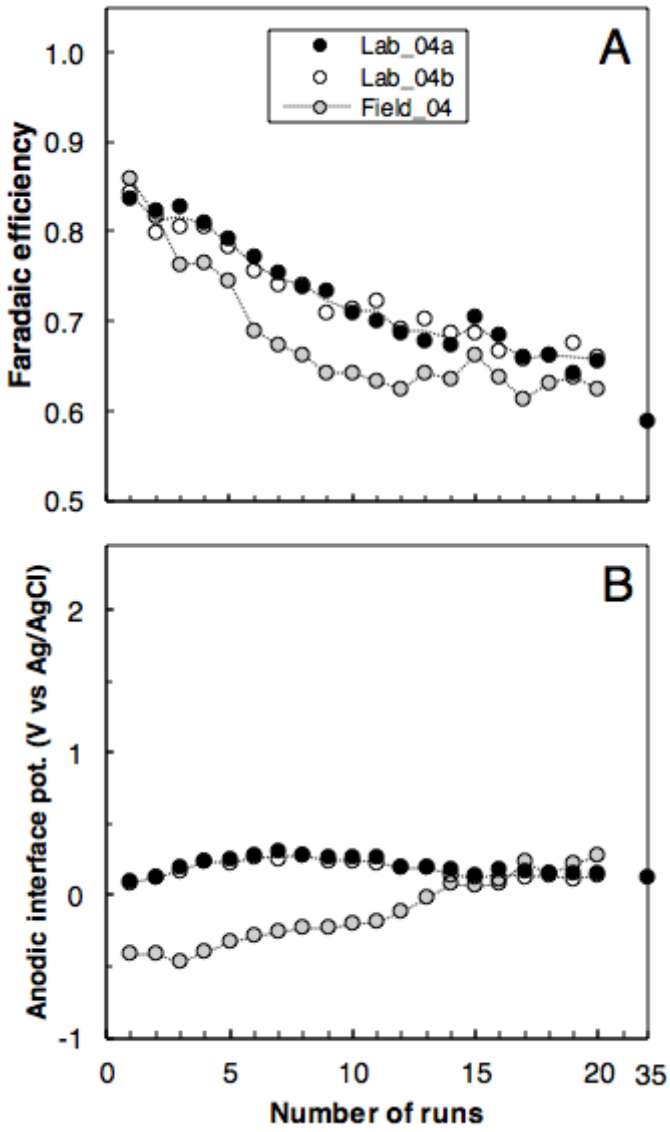

Figure 2. Faradaic efficiency (A) and anodic interface potential (B) as a function of the number of runs for experiments performed at *CDR* of 4 C/L/min in SGW. The experiments with laboratory Fe electrodes (black filled circles and open circles) were performed as duplicates. A piece of steel from the field reactor (Amrose et al. 2014) with a lower purity was used as anode for Field_04 (grey filled circles). The *FE* and the interface potential of Lab_04a after 35 runs are indicated. Additional parameters are summarized in Table 3.

3. Results

3.1 Laboratory and field anodes

3.1.1 Faradaic efficiency

Figure 2A shows the behavior of the Faradaic efficiency (*FE*) for the laboratory steel anode replicate experiments (Lab_04a & b as duplicates) and the field steel anode (Field_04) experiment at a charge dosage rate (*CDR*) of 4 C/L/min in SGW. For all three experiments, the Faradaic efficiency (*FE*) started below 1 and decreased over time, i.e. less Fe was present in the bulk solution than expected based on Faraday's law. Starting at a *FE* of 0.85 (85 % of the charge was converted to Fe in the bulk solution), the laboratory anodes showed a gradual reduction in *FE* to 0.66 over 20 runs, which includes electrolysis and storage open to the atmosphere between runs. These results were reproducible, as the *FE* of the duplicates behaved almost identical over the entire 20 runs. Although we only present the final data point in Figure 2 for experiments with total run numbers above 20, the *FE* for Lab_04a continued to decrease over 35 runs, the longest continuous experiment in this work, and reached a minimum near 0.6.

The *FE* of the field anode over time was similar to the laboratory anodes, but decreased to 0.62 after 20 runs, which is equal to a final Fe dose of approximately 80 mg/L. The similarity in *FE* between the field and laboratory electrodes suggests that a high purity Fe electrode does not necessarily translate to sustained high *FE* at the investigated *CDR* of 4 C/L/min.

3.1.2 Anode interface potential

The corresponding behavior of the anodic interface potential (*IP*) over the same number of runs is shown in Figure 2B. The experiments with lab anodes began at *IP* close to 0 V vs Ag/AgCl and increased slightly to 0.2 V vs Ag/AgCl during the first 10 runs. Despite a continuously decreasing *FE*, the *IP* for Lab_04a remained stable over the entire 35 runs and no differences in *IP* were observed between the duplicates. The field anode had a lower initial *IP* (- 0.4 V vs Ag/AgCl), but increased almost linearly throughout the 20 runs, resulting in a higher final *IP* (0.3 V vs Ag/AgCl) than measured for the laboratory anodes.

3.1.3 Surface layer formation

The formation of electrode surface layers (SL) was observed under all experimental conditions on both anodes and cathodes. We present the visual differences among these layers, their quantities, and the results from XRD analysis separately for anodes and cathodes for each group of experiments.

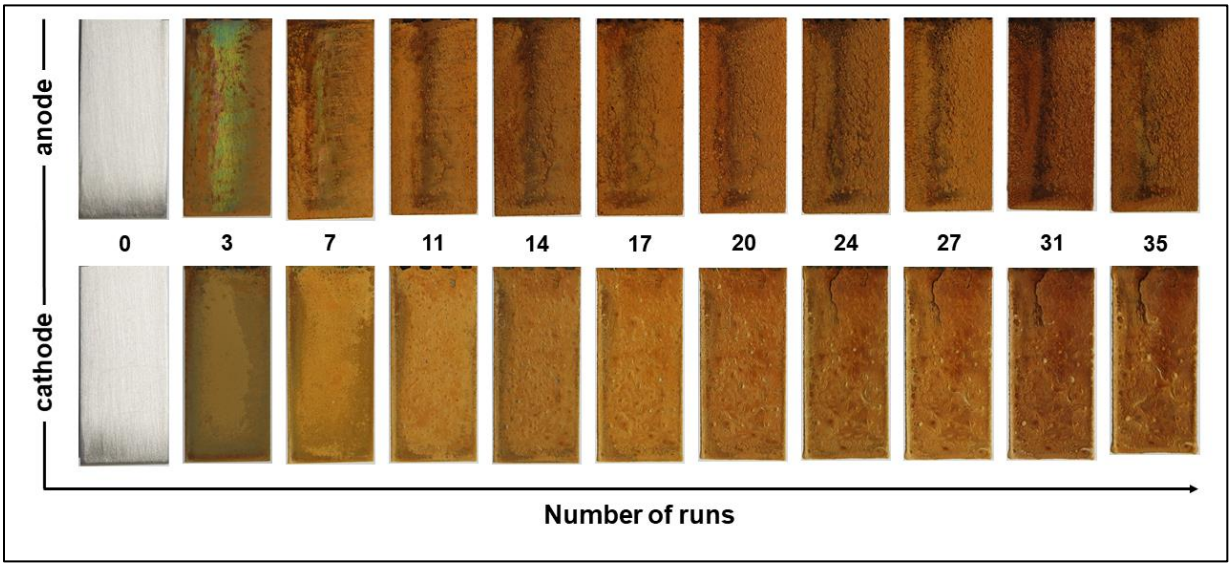

Figure 3. Surface layer formation on the anode and cathode of experiment Lab_04a.

The changes of the anode and cathode surface of experiment Lab_04a over 35 runs is shown in Figure 3. On the anode, the onset of a layer was observed after the first run, and the metallic steel surface completely disappeared after approximately 8 runs. Their colors are diverse and best described as orange hues (2.5 Yellow-Red in Munsell color system) over a wide range of chroma and value. Over 35 runs, the layer developed a rough surface and the colors became darker (lower values). In the middle and the top of the anode, where the layer remained thinner, the SL became black. Similar macroscopic surface layers were observed on the electrodes of experiment Lab_04b and Field_04, which operated under the same conditions (Annex Figure 4), suggesting the purity of the electrode does not impact the macroscopic properties of the surface layers.

The SL of Lab_04b and Field_04 was removed with a brass brush after 20 runs. A smaller quantity was removed from the surface of the field anode (0.6 mg/cm^2) relative to the

laboratory anode (1.8 mg/cm^2). Applying the same technique after 39 runs on the electrodes of Lab_04a removed only 1.6 mg/cm^2 from the anode.

The results of powder XRD analysis of electrode SLs from Lab_04b and Field_04 show that the anode and cathode SLs consist of completely different mineral phases (Annex Figure 2). The results for the anodic layers indicate that crystalline Fe (oxyhydr)oxide phases are not present in substantial fractions. The broad peaks around 35° suggest a ferrihydrite-like, poorly ordered Fe(III) precipitate (Schwertmann and Cornell 2000). No XRD peaks related to the presence of goethite, lepidocrocite, or other Fe(II,III) minerals common in corrosion layers were identified.

The cathode of experiment Lab_04a was covered by a homogenous orange layer (5YR 6/10) after 3 – 7 runs. Over 35 runs, the SL became darker and patchy with notable white spots. In contrast to the anode, the cathodic layer became brittle, cracks were observed, and small parts of the cathodic layer were lost during electrolysis. Similar macroscopic SLs were also observed on the cathodes of experiment Lab_04b and Field_04 (Annex Figure 4).

Compared to the anodes, a bigger quantity was removed from cathodes after 20 runs, 6.6 and 6.8 mg/cm^2 (Lab_04b and Field_04). The mass removed per cathode area from Lab_04a after 39 runs was even higher (10.9 mg/cm^2).

The XRD patterns of the cathodic SL show that calcium carbonates, i.e. calcite and aragonite, are the major crystalline phases of these SLs. Although no evidence for crystalline Fe mineral phases appeared in the XRD of these cathodic SLs, the brownish color and the detection of Fe by wet chemical methods in the surface layer suggest the presence of a fraction of poorly crystalline Fe(III) precipitates.

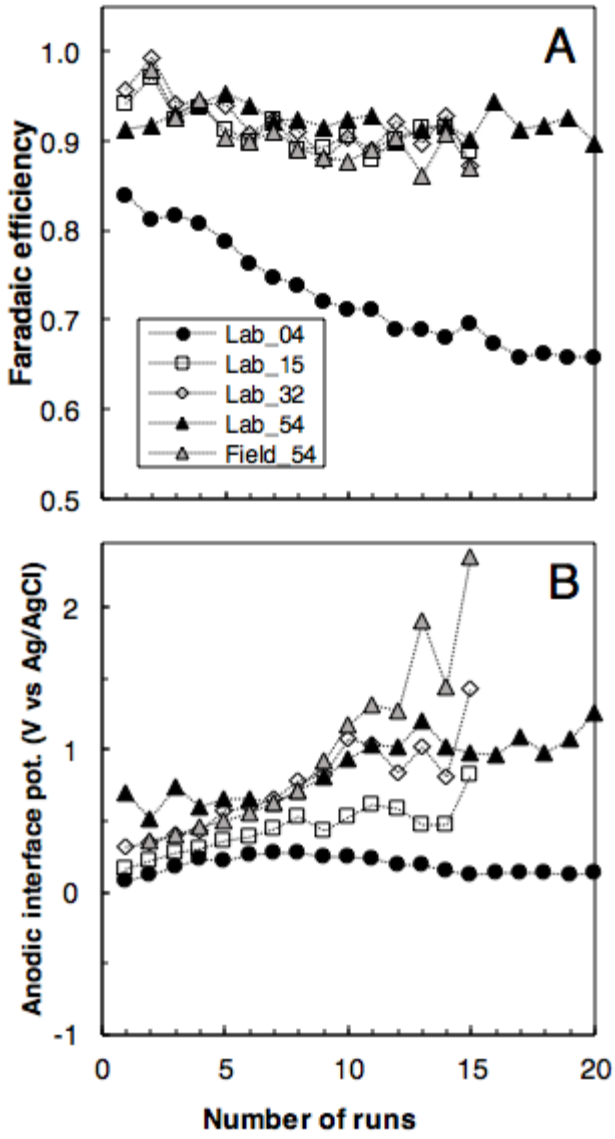

Figure 4. Faradaic efficiency (A) and anodic interface potential (B) as a function of the number of runs for experiments performed in SGW at different charge dosage rates. Lab electrodes were used in all experiments except Field_54. The average of Lab_04a & b is given. The different *CDR* of each experiment is reflected in the name, i.e. Lab_54 conducted at 54 C/L/min. Additional parameters are summarized in Table 3.

3.2 Impact of charge dosage rate

3.2.1 Faradaic efficiency

Figure 4A shows the impact of the *CDR* on the *FE* over 15 to 20 runs. The long-term *FE* of experiments at elevated *CDR* were clearly above the *FE* of the reference experiments (average of Lab_04a & b) performed at *CDR* of 4 C/L/min. At *CDR* ≥ 15 C/L/min, the *FE* of the first run was between 0.9 – 0.96, which is substantially higher than the *FE* of the first experiment at *CDR* 4 C/L/min (*FE* = 0.84). Furthermore, the *FE* at elevated *CDR* remained above 0.85 throughout the entire 15 to 20 runs. Remarkably, no differences in long-term *FE* were observed between the different experiments at elevated *CDR* (15, 32, 54 C/L/min) and between the field and lab anode at high *CDR*. This trend contrasts that of the low *CDR* experiments, which decreased continuously over 20 runs, and eventually led to a *FE* difference of 0.24 between the high and low *CDR* experiments.

3.2.2 Anode interface potential

The effect of *CDR* on the *IP* is illustrated in Figure 4B. We observed that the *IP* of the initial runs increased with increasing *CDR*, which is consistent with the Butler-Volmer relationship (Bard and Faulkner 2001). Furthermore, in contrast to the stable *IP* of Lab_04, the *IP* of experiments at elevated *CDR* increased with the number of runs. This trend is particularly true for the experiment with the field anode at high *CDR*, which was below 0.5 V vs Ag/AgCl at the first run and reached above 2 V vs Ag/AgCl after 15 runs. Despite an *IP* above 2 V vs Ag/AgCl, a high *FE* was maintained for experiments at elevated *CDR*, which indicates that the production of Fe(II) was the dominant reaction on the anode.

3.2.3 Surface layer formation

Consistent with the dependence of the *FE* on the *CDR*, the macroscopic properties of the electrode SLs depended strongly on the *CDR*. (Annex Figure 3 and 4). For experiments at *CDR* > 15, only small quantities were removed from anodes (0.2 mg/cm^2) and the SL was much darker compared to the experiments at a *CDR* of 4 C/L/min. Powder XRD could not be used to identify the mineral phases on the surface of anodes at *CDR* > 15 due to insufficient quantities removable by mechanical brushing. Chemical extraction showed that the ratio of Fe on the anode/cathode was above 10 for all experiments at elevated *CDR,* which is consistent with the detection of Fe minerals on the anode and mainly calcite on the cathode at low *CDR* in SGW.

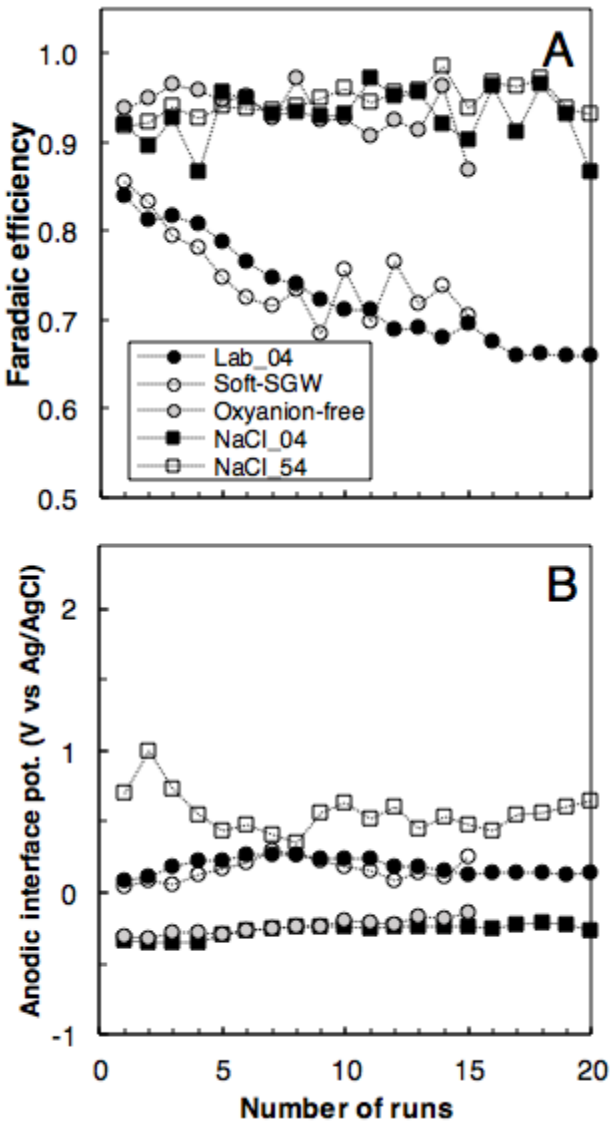

Figure 5. Faradaic efficiency (A) and anodic interface potential (B) as a function of the number of runs for experiments performed with lab electrodes in electrolytes of different composition. SGW was used for Lab_04 (black filled circles, average of Lab_04 a & b). Soft-SGW (open circles) and oxyanion-free-SGW (grey filled circles) were compared to a 10 mM NaCl (filled squares) at *CDR* of 4 C/L/min. In addition, the NaCl electrolyte was also tested at *CDR* of 54 C/L/min (open squares). Additional parameters are summarized in Table 3.

On the cathodes, a brighter layer developed (orange hues like 10YR 8/8 at center, almost white at margins) and none of the macroscopic cracks observed on the cathode for *CDR* = 4 C/L/min experiments were found.

3.3 Electrolyte composition effects

3.3.1 Faradaic efficiency

Figure 5A shows that the composition of the electrolyte played a critical role in the behavior of the *FE*. A stable *FE* above 0.9 was observed over all runs in electrolytes containing only NaCl or SGW free of oxyanions (Oxyanion-free), regardless of the low *CDR* used in these experiments. When oxyanions (HPO_4^{2-}, SiO_3^{2-}, and HCO_3^-) were present in the electrolyte, the decrease in *FE* with the number of runs was similar in the presence and absence of Ca and Mg (Soft-SGW and regular SGW), suggesting that bivalent cations do not impact considerably the processes affecting Fe(0) oxidation and

release during Fe(0) EC. Increasing the *CDR* in NaCl electrolyte did not increase the *FE* further like in SGW, it was already high at low *CDR* in NaCl.

3.3.2 Anode interface potential

The *IP* depended strongly on the electrolyte composition (Figure 5B). Consistent with the *FE* behavior, the absence of Mg and Ca did not change the *IP* compared to SGW. However, a significantly lower *IP* (around – 0.25 V vs Ag/AgCl) was observed when oxyanions were absent. In agreement with our previous observations for experiments in SGW, increasing *CDR* also increased the initial *IP* in 10 mM NaCl electrolyte, but the same increase in *IP* over 20 runs observed in SGW was not found for experiments in the NaCl electrolyte.

3.3.3 Surface layer formation

In addition to impacting the *FE*, the electrolyte composition also altered the electrode SLs (Annex Figure 5). In oxyanion-free SGW, the SL was darker and more reddish (10R 4/10) compared to Lab_04. Only 0.3 mg/cm^2 could be removed mechanically, which was not sufficient for characterization by powder XRD. When Ca and Mg were absent (Soft-SGW), an anodic layer with orange hues (2.5YR) and a quantity (1.8 mg/cm^2) similar to Lab_04 was observed. This anode layer was found to be ferrihydrite-like by XRD (Annex Figure 2). For both experiments at 4 and 54 C/L/min in the 10 mM NaCl electrolyte, similar orange anodic SLs were observed (10R 5/12 with black dots), but the SL mass removed was higher at low *CDR* (1.2 compared to 0.2 mg/cm^2). For experiments performed in the NaCl electrolyte, lepidocrocite was the major phase found in the anodic SLs (Annex Figure 2).

The effect of electrolyte composition on cathode SLs was different. In Oxyanion-free SGW, the SL mass removed from the cathode was much higher (6.2 mg/cm^2) compared to the anode. Distinct from experiments at the same *CDR* in SGW, the cathodic layer was more heterogenous and did not show any cracks. When Ca and Mg absent, which prevented calcium carbonate from forming, no continous cathodic layer was observed. Instead, an irregular orange pattern formed on the cathode (0.7 mg/cm^2). Similar to the anode, a ferrihydrite-like phase was present on the cathode (Annex Figure 2). In NaCl electrolyte, black SLs were formed on the cathodes independent of the applied *CDR*. However, the SL mass was higher at low *CDR* (1.6 compared to 0.8 mg/cm^2). In both experiments performed in the NaCl electrolyte, magnetite dominated the cathodic SL (Annex Figure 2).

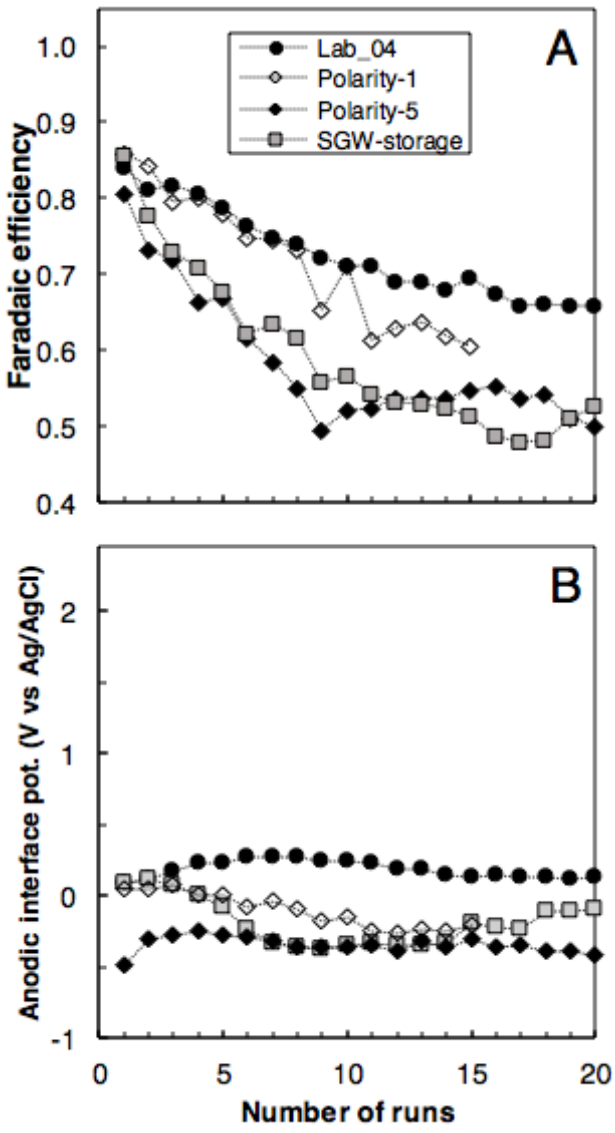

Figure 6. Faradaic efficiency (A) and anodic interface potential (B) as a function of the number of runs for experiments performed with lab electrodes in SGW at 4 C/L/min. Unlike the reference experiments (black filled circles, average of Lab_04a & b), the polarity was changed between the runs (open diamonds, Polarity-1) and between runs and four times during electrolysis (black filled diamonds, Polarity-5. The electrodes of experiment SGW-storage (grey filled squares) were stored in SGW instead of open to the atmosphere. Additional parameters are summarized in Table 3.

3.4 Polarization alteration and electrode storage

3.4.1 Faradaic efficiency

Alternating electrode polarities and water saturated storage were tested as potential strategies to improve long-term *FE*. Figure 6A shows that alternating the polarity and storing the electrodes in SGW rather than open air both decreased strongly the FE. Polarity reversal between every run resulted in a decreasing FE similar to the experiments without polarity reversal (Lab_04) until run number 10. After run 10, the *FE* of polarity switching experiments was consistently lower than without polarity reversal. Alternating the polarity several times during one run resulted in a much faster decrease in *FE* below 0.5 where it remained for the rest of the long-term experiment. A similar trend, a quick decrease and a stable *FE* around 0.5, was also observed for the water saturated storage conditions without polarity reversal. Evidently, neither potential strategy for improving the long-term *FE* proved effective.

3.4.2 Anode interface potential

All three experimental conditions also lead to a lower interface potential compared to Lab_04 (Figure 6B). The initial *IP* of Polarity-1 and SGW-storage was similar to Lab_04 and decreased below 0 V vs Ag/AgCl after four runs. The interface potential of experiment Polarity-5, however, did not change with time, and remained around - 0.4 V vs Ag/AgCl over the entire 20 runs.

3.4.3 Surface layer formation

Alternating the polarity had a strong effect on the formation of macroscopic surface layers. A brittle layer similar to the cathodic layers of Lab_04 was formed on both electrodes, which is

consistent with both electrodes serving as cathode 50% of the time. The dominant phase on the surfaces of Polarity-1 and Polarity-5 electrodes was calcite. However, in contrast to the cathodic layers of other experiments in SGW, magnetite was also detected (Annex Figure 2). This result is in agreement with previous extended field trials of Fe-EC systems, which reported electrode layers containing magnetite and calcite. The formation of cracks was observed on electrodes of both polarity experiments, but the cracks were more visible at the surface of Polarity-5. Although parts of these layers were lost to the bulk electrolyte during electrolysis, an average mass of 7.2 mg/cm^2 (Polarity-1) and 10 mg/cm^2 (Polarity-5) were removed from each electrode after 15 and 20 runs, respectively.

The electrodes stored in SGW showed the heaviest of all surface layers (20 mg/cm^2 on the anode after drying). The anodic layer was dark orange in color and had an uneven surface. Powder XRD revealed the mineralogy of the layer was similar to the anodes stored open to the atmosphere (Lab_04). Calcite was also detected on the anode and cathode, but was the major phase on the cathodic layer, even though the cathode had a much darker color compared to Lab_04. A poorly crystalline ferrihydrite-like phase was identified as the major phase present on the anode (Annex Figure 2).

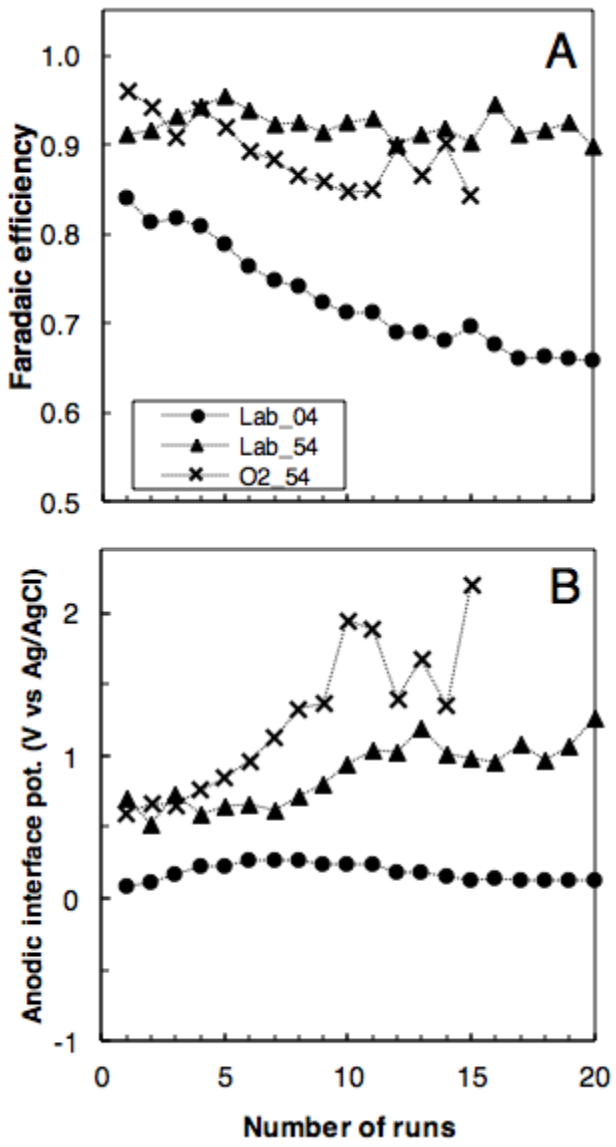

Figure 7. Faradaic efficiency (A) and anodic interface potential (B) as a function of the number of runs for experiments performed with lab electrodes in SGW at high *CDR* (54 C/L/min, crosses and triangles) and low *CDR* (4 C/L/min, circles). The solution of O2_High was aerated to maintain high oxygen concentrations in contrast to Lab_54, where oxygen concentrations dropped < 0.1 mg/L at the end of electrolysis. Additional parameters are summarized in Table 3.

3.5 The role of oxygen

3.5.1 Faradaic efficiency

Because we observed a higher *FE* in experiments at *CDR* ≥ 15 C/L/min, accompanied by a much lower O_2 concentration in the electrolyte, the aim of experiment O2_54 was to examine if the dissolved oxygen concentration rather than *CDR* affected the long-term FE. Figure 7 compares the performance of lab electrodes at a *CDR* of 54 C/L/min with additional aeration (O2_54) to the standard setup without aeration (Lab_54).

Only minor differences were observed between Lab_54 and O2_54. Starting at a *FE* of 0.96, the *FE* of the aerated system decreased over the first 10 runs and reached a minimum at 0.85. The *FE* of the following runs was less stable and between 0.84 and 0.9. Without aeration, a more stable *FE* around 0.9 was achieved over the entire 20 runs. Compared to the loss in *FE* over the same number of runs at low *CDR* (Lab_04), the *FE* of O2_54 was consistently higher, indicating that (low) oxygen concentrations are not the main reason for the higher *FE* at *CDR* ≥ 15 C/L/min.

3.5.2 Anode interface potential

The initial *IP* of both experiments was approximately 0.7 V vs Ag/AgCl and increased with the number of runs. The *IP* of O2_54 increased over the first 10 runs and reached a maximum around 2 V vs Ag/AgCl, whereas the IP of Lab_54 showed a gradual increase and reached a maximum around 1.1 V vs Ag/AgCl after 13 runs. These results show that although bubbling O2 did not impact considerably the FE of the CDR_54 experiments, the presence of elevated O2 concentrations did impact the IP.

3.5.3 Surface layer formation

The macroscopic surface layer that formed on the anode of O2_54 had a color similar to the anode of Lab_54 (Annex Figure 4). However, the SL in the aerated system was heavier (0.8 mg/cm^2 compared to 0.2 mg/cm^2), despite the fewer number of runs. The mineral phases in the anodic layer of O2_54 were characterized as ferrihydrite-like precipitates and lepidocrocite (Annex Figure 2), whereas no lepidocrocite was detected in the SL of Lab_04. The cathodic layers were not analyzed with powder XRD, but the white precipitates indicated the presence of calcium carbonates.

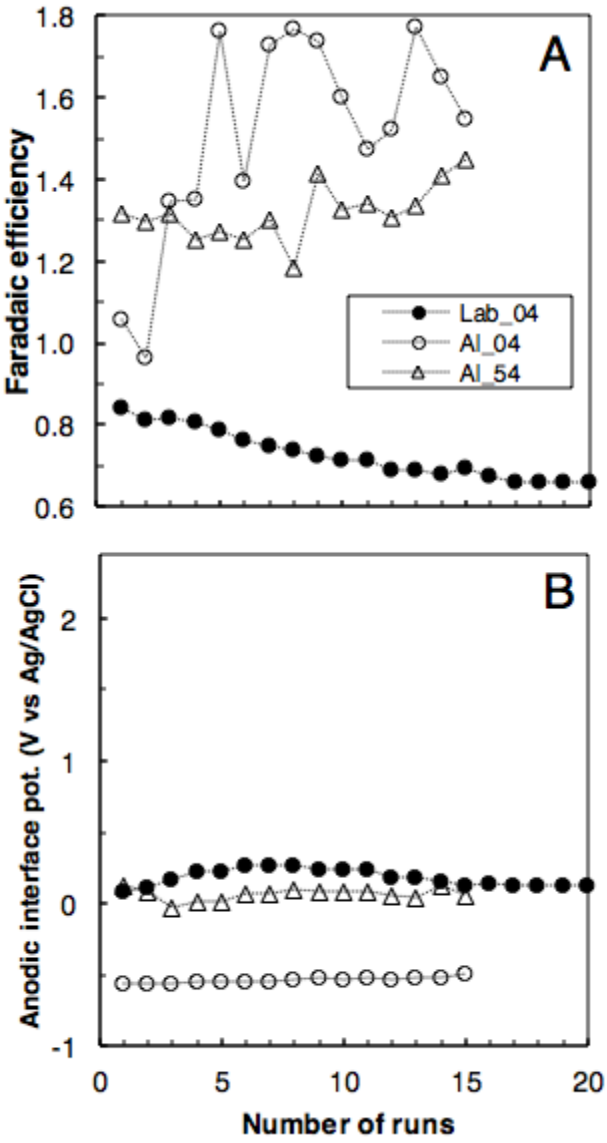

Figure 8. Faradaic efficiency (A) and anodic interface potential (B) as a function of the number of runs for experiments performed with in SGW. The reference experiments with lab Fe electrodes (black filled circles, average of Lab_04a & b) were conducted at 4 C/L/min. Aluminum electrodes were used for Al_04 (open circles) at 4 C/L/min and for Al_54 (open triangles) at 54 C/L/min. Additional parameters are summarized in Table 3.

3.6 Behavior of Al electrodes

3.6.1 Faradaic efficiency

Figure 8A shows the performance of Aluminum electrodes operated at different *CDR* in SGW. In contrast to all Fe electrode experiments, the measured Al concentrations were higher than predicted by Faraday's law (n = 3 for Al(0) electrolysis), resulting in *FE* values above 1. Operated under the same conditions as Lab_04, the *FE*, starting around 1, increased to values above 1.6 but showed large fluctuations between runs. This unique behavior of Al(0) electrodes is likely attributed to the different electrochemical behavior of Al(0) compared to Fe(0) and is consistent with previous Al-EC studies (Mechelhoff et al. 2013). When a *CDR* of 54 C/L/min was applied, the *FE* was relatively stable, starting at 1.3 and increased to 1.4 after 15 runs. This result might be explained by the lower contact time of the Al(0) electrodes with the electrolyte in the high *CDR* experiments, leading to less passive Al(0) corrosion, which is not taken into account in calculations of the *FE*.

3.6.2 Anode interface potential

The interface potential was very stable at - 0.5 V (Al_Low) and 0 V (Al_High). The *IP* of Al electrodes did not exceed the potential measured at Fe electrodes (Lab_04), indicating that there is

a major difference in the electrochemical properties of Al(0) and Fe(0).

3.6.3 Surface layer formation

Macroscopic surface layers were formed on all Al electrodes, but were very different in quantity and structure (Annex Figure 7). At low *CDR* (Al_04), both cathodic and anodic layers were massive (11.7 and 10.5 mg/cm^2, respectively), whereas at high *CDR* (Al_54), SLs with a much lower mass were formed (1.8 and 0.6 mg/cm^2).

3.7 EC product formation

Fe precipitates, very different in color and size, were formed in the EC cell when electrolyte composition, *CDR*, dissolved O_2 concentration were varied (Annex Figure 3 – 6). The structure of the precipitates was not analyzed in this study, however, based on previous studies, we state the possible major mineral phases formed during electrolysis.

In all experiments in SGW at *CDR* = 4, the electrolyte turned turbid and small orange precipitates were formed, most likely nanocrystalline Fe(III) (oxyhydr)oxides with a structure similar to ferrihydrite (van Genuchten et al. 2012). Increasing the *CDR* in SGW decreased the fraction of small orange Fe precipitates and large blue-green flocs were generated, most likely carbonate green rust (Dubrawski et al. 2015). When oxygen concentrations > 3 mg/L were sustained at high *CDR* (O2_54), the Fe-precipitate appeared similar to the precipitates formed at a *CDR* of 4 C/L/min (Lab_04). While no precipitates remained on the glass beaker surface at the end of electrolysis, Fe-precipitates remained at the air dispenser of O2_54 and were removed with HCl before the following run. These effects were independent of the Fe(0) anode purity, polarity alternation, or electrode storage.

The electrolyte composition affected the Fe precipitates formed during electrolysis. In Soft-SGW, an orange precipitate similar to Lab_04 was formed. In oxyanion-free SGW, a more reddish and less turbid product with visible flocs was generated. Both suspensions in modified SGW did not settle completely, in contrast to the precipitates generated in SGW. In NaCl electrolyte, large orange flocs were formed at a low *CDR*, most likely lepidocrocite (Dubrawski et al. 2015). By contast, at high *CDR* (NaCl_54), small black particles with magnetic properties were generated, most likely magnetite (Dubrawski et al. 2015).

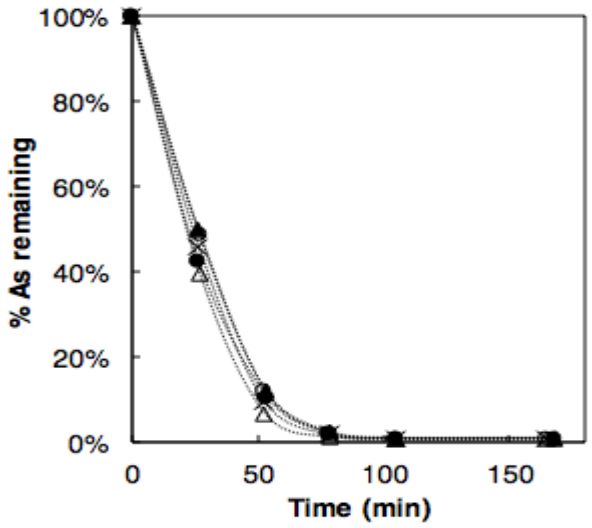

Figure 9. As removal experiments before (filled symbols) and after mechanical cleaning and HCL wash (open symbols). The initial As(III) concentrations (640 µg/L) were decreased below detection limit under all conditions, resulting in a removal efficiency of 99 %. Electrodes from Lab_04b with high purity steel (circles), Field_04 with the field anode material (triangles), and unused steel electrodes as reference (cross) were used.

3.8 Arsenic removal

To evaluate the arsenic removal efficiency under realistic conditions (surface layer after 19 runs), As contaminated SGW was used during run number 20 in experiment Lab_04b and Field_04. After the experiment, the SL was mechanically removed, the electrodes were cleaned with HCl and sandpaper, and the experiment was repeated.

No significant differences were observed at the chosen total charge dosage of 450 C/L, which is identical to the total dose applied in the field system (Figure 9). Arsenic was removed to below detection limit under all conditions (equivalent to at least 99 % removal of As(III)). Additional aeration at the end of electrolysis had no effect on As removal under these conditions. The lack of significant differences can be explained by the amount of Fe generated in these experiments, which is far more than required to remove 640 µg/L As.

3.9 Modifications to enhance Faradaic efficiency

Figure 10 shows the Faradaic efficiency and interface potential for Lab_04a over the last 7 runs. Different modifications were tested at run number 36, 38, and 40, always followed by one run under reference conditions (*CDR* = 4 C/L/min, SGW). These modifications, which are delineated by A), B), and C) in Figure 10, were applied to test if the *FE* was improved in the following standard experiment and are explained below.

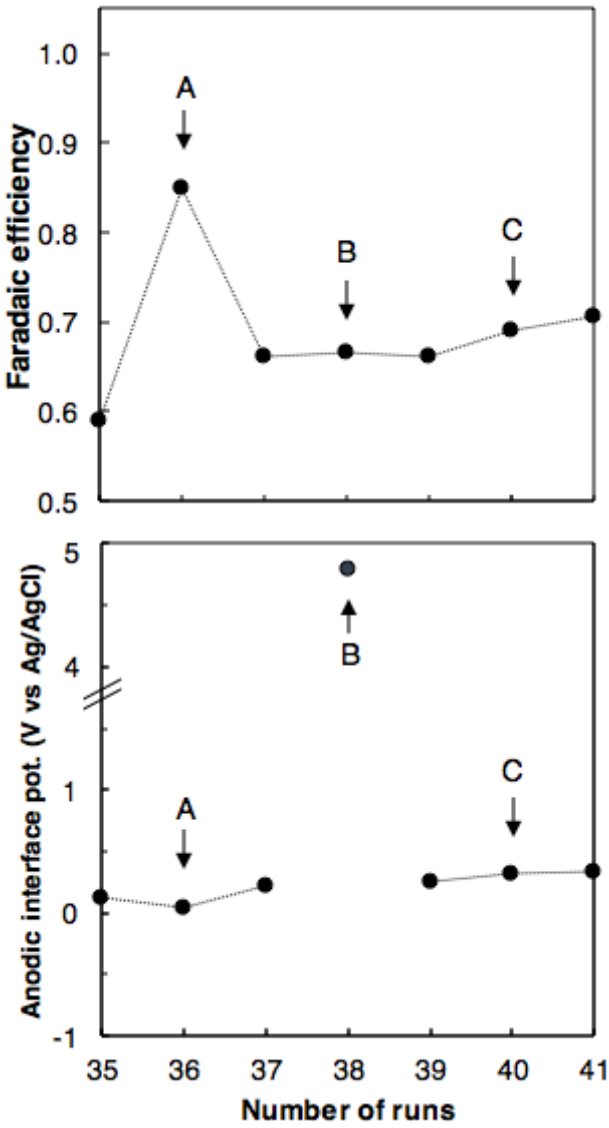

Figure 10. Results from experiment Lab_04a as a function of the number of operations (run 35 – 41) with lab electrodes in SGW at a *CDR* of 4 C/L/min. Faradaic efficiency (top panel) and the anodic interface potential (bottom panel). Different modifications were tested at the end of the experiment: A. addition of 2 mL lemon juice, B. high charge dosage rate (54 C/L/min), C. light brushing with a brass brush.

A. Lemon juice (2 mL filtered over 0.45 μm) was added before the experiment, which decreased the initial pH below 6 and increased the *FE* to 0.85, similar to the initial *FE* observed at run 1. The interface potential was not affected during the lemon juice amendment. However, the following run under normal conditions showed a *FE* significantly higher than before lemon juice addition (12 % increase in Fe dose).

B. The charge dosage rate was increased to 54 C/L/min. However, no constant current could be supplied in the first 1.5 min due to the very high initial cell voltage (> 30 V). The *FE*, calculated for a constant current, did not decrease, but the interface potential was almost 5 V vs Ag/AgCl. The following run at a low *CDR* led to a similar *FE*.

C. The electrode surfaces (anode and cathode) were brushed with a soft brass brush prior to the experiment. This removed major parts of the cathodic layer but only a fraction of the much more robust anodic layer. The *FE* increased slightly (5% increase in Fe dose) compared to the value before brushing and the *IP* did not change. Based on these results, soft brushing did not improve significantly the *FE*.

4. Discussion

4.1 Comparison between extended laboratory and field system operation

One of the main aims of this study was to evaluate the long-term *FE* of Fe-EC systems in controlled experiments that mimicked field Fe-EC systems. We expected that the *FE* would decrease when the EC system is operated under conditions close to the field system, namely a *CDR* of 4 C/L/min, low-purity steel anodes, a synthetic groundwater electrolyte, polarity reversal between each run, and the storage of electrodes open to the atmosphere.

The hypothesis was confirmed for all conditions to test typical field operation (Lab_04, Field_04, Polarity-1). Surprisingly, the lower purity of the field anode (Field_04) did not affect the long-term *FE* compared to the laboratory anodes (Lab_04). Polarity reversal between runs (Polarity-1) decreased the long-term *FE* compared to the anode-cathode system (Lab_04).

4.1.1 Similarities between the field system and our study

In the field Fe-EC system, the *FE* was not tracked, which is the reason why we mimicked the system in the laboratory. Instead, other observations and measurements made by Amrose et al. (2014) and van Genuchten et al. (2016) will be compared to our experimental results.

Similar to the field system, iron-rich macroscopic layers were formed on the electrodes, which suggests that oxidized Fe was trapped and decreased the *FE* over extended operation. XRD analysis of the field SLs revealed magnetite, calcite, and goethite. Similarly, calcite and magnetite were detected in SLs from our Polarity-1 experiment, which mimicked field operation including polarity change between runs. The presence of goethite and the fact that magnetite was the major phase detected in field SLs might be explained by the longer operation of the field system (> 100 compared to 15 runs). Longer operation might favor magnetite formation by trapping of Fe(II) in the SL (van Genuchten et al. 2016) and, over time, the transformation of poorly crystalline Fe minerals to goethite can occur (Cornell and Schwertmann 2003).

A striking difference between field and lab system are the colors of the electrodes. In the field system, electrode colors alternated (orange and grey), whereas both electrodes of Polarity-1 appeared identical (orange). We expect that the alternating colors of field electrodes are due to formation of different mineral phases during one run.

In both systems, field and lab, parts of the SL chipped from the electrode. Because such a behavior was not observed on fixed anodes, we attribute it to the polarity alternation. Therefore, the Polarity-1 experiment is closest to the field system. The observed continuous decrease in *FE* (Figure 6, Polarity- 1) reaching 0.6 after only 15 runs has important implications for the operation of the field-EC system.

4.1.2 Reasons for a low *FE* under field-like conditions

A low *FE* can originate from two main reasons, limited Fe(II) generation due to competing side reactions (e.g. oxidation of water) or the produced Fe(II) does not end up in the bulk electrolyte.

Ideally, we would answer the question with a Fe mass balance: Fe that did not end up in the bulk electrolyte is either incorporated in the SL or was not generated due to side reactions. Unfortunately, both SL quantification methods (chemical Fe extraction and mechanical removal) had drawbacks and their results are not suitable for a Fe mass balance. We recommend measuring the Fe content of the Polarity-1 SL, which could be removed successfully in contrast to the anodic layers.

Instead, we will discuss the possible reasons that resulted in the decrease in *FE* over repeated operation. Reactions on the anode competing with Fe oxidation, like the oxidation of water, are often reported for Fe-EC (Mollah et al. 2004), but recent studies indicate that other reactions than Fe oxidation happen only at interface potentials above 1.5 V vs Ag/AgCl (van Genuchten et al. 2017). We observed a maximum *IP* of 0.4 V vs Ag/AgCl under field-like conditions, indicating that such reactions are not responsible for the observed decrease in *FE*. Nevertheless, the *IP* was measured at only one location on the anode and higher potentials might occur locally.

The formation of iron-rich SLs suggests that a fraction of generated Fe(II) did not end up in the bulk electrolyte. Different mechanisms for SL formation and growth have been proposed in the literature: For instance, Fe(II) could remain on the anode and be trapped by an existing SL (van Genuchten et al. 2016). However, Fe(II) minerals containing Fe(II) (magnetite) were only detected in experiments with polarity reversal, whereas in experiments with fixed anodes poorly crystalline Fe(III) phases were detected. Still, magnetite might also be present in the anode SL, but was not removed by brushing, as a visible oxidized layer remained on anodes. In contrast, the brittle SL that formed when polarities were reversed was much easier to remove. Other authors proposed that Fe precipitates could be deposited on the electrode surface, but would be inhibited by high flow velocities (Timmes et al. 2010). Indeed, the partial layer that was observed after three runs (Figure 3) is likely to be caused by higher flow velocities in the middle of the electrode. In addition, similarities between layer structure (poorly crystalline Fe precipitates) and the expected precipitates in the bulk electrolyte could indicate that deposition takes place.

Cathodic layer formation is different relative to the anodes, as we observed primarily calcite SLs in our SGW electrolyte with a similar composition as natural groundwater in Bangladesh. Calcite formation can be explained by the locally high pH at the cathode-electrolyte interface due to cathodic OH^- production (Lakshmanan et al. 2009). However, it is important to note that the cathodic layers also contained iron, which can only originate from Fe precipitates deposited on the cathode from the bulk electrolyte. Therefore, both anodic and cathodic SLs contribute to the low *FE* observed under field conditions.
Polarity alternation, however, resulted in a lower *FE* and SLs similar to the cathodic calcite layers. It is striking that when calcite was present, the SL and the steel surface were not strongly bound, in contrast to robust, coherent SLs on fixed anodes. Also the lower *FE* in experiment Polarity-1 might be a result of the unstable SL. During the first runs, switching the polarity between each run did not result in a lower FE compared to fixed anodes/cathodes. Therefore, the presence of calcite on the

anode surface alone did not decrease the *FE* directly. The drop in *FE* of Polarity-1 compared to Lab_04 coincided with the formation of visible cracks in the SL. The rapid decline in *FE* of experiment Polarity-5 was accompanied by distinct crack formation in the SL, possibly caused by $H_{2(g)}$ bubble formation. We expect that calcite precipitation and crack formation increased the effective surface area of the SL, which trapped more Fe than SLs formed on fixed anodes and cathodes.

We described the similarities between the Fe-EC system in the field and in the laboratory and elucidated potential reasons for the decreasing *FE* in these Fe-EC systems. We found that SL formation is likely to play an important role, but the key parameters that govern the *FE* remained unclear. Consequently, other variables such as the applied *CDR* or the electrolyte composition are key to understand the behavior of *FE* over time and will be evaluated in more detail in the following sections.

4.2 Factors affecting *FE*

We observed two major trends in Fe generation when the laboratory system was operated for 15 – 35 runs: (i.) We found that the Faradaic efficiency (*FE*) declined for experiments at low *CDR* (4 C/L/min) and in electrolytes rich in oxyanions. (ii.) We observed two conditions that resulted in a higher and more stable *FE*: a *CDR* ≥ 15 C/L/min in SGW **or** oxyanion free electrolytes at any *CDR*.

Correlated to the decreased *FE*, we observed the formation of macroscopic layers on the surface of the electrodes under experimental conditions that produced low *FE*, including the experiments discussed in the previous section. By contrast, low-mass surface layers formed in most systems with a higher *FE,* e.g. high *CDR* and oxyanion-free electrolytes. Despite the formation of some macroscopic surface layers, we did not observe the complete inhibition of Fe oxidation (i.e. anodic passivation) in any experiment. In the following sections, we discuss these observations and elucidate the implications of our results for the operation of EC field systems.

4.2.1 Higher *FE* at elevated *CDR*

We observed that a *FE* above 0.8, often above 0.9, was maintained for all experiments at *CDR* ≥ 15 in SGW. Surprisingly, also the *FE* of the first run was higher than at low *CDR*. By changing the *CDR*, a number of variables of the Fe-EC system are affected, which will be evaluated in the following.

Anode interface potential. By increasing the *CDR*, the current density and the *IP* were increased, which is consistent with the Butler-Volmer equation (Bard and Faulkner 2001). The higher *IP* could favor competing anode reactions, which would decrease *FE*. Instead, we observed the opposite, a high long-term *FE* at *CDR* between 15 and 54 C/L/min. Only in two experiments (Field_54, O2_54), a slightly lower *FE* at single runs might originate from *IP* > 1.5 V vs Ag/AgCl. Consequently, a *CDR* between 15 and 54 C/L/min is unproblematically concerning oxidation reactions that could occur at higher *IP*.

Reactive O_2 species. In all experiments at elevated *CDR*, oxygen consumption by Fe(II) oxidation exceeded the influx of O_2, which resulted in O_2 concentrations close to 0 mg/L at the end of electrolysis. During the oxidation of Fe(II) by O_2, reactive oxygen intermediates such as superoxide radical are produced (Hug and Leupin 2003). If we increase the *CDR*, the production of reactive O_2 species itself might be lower due to low O_2 concentrations. Also, the loss of reactive O_2 species by reactions with Fe(II) is more likely due to higher Fe(II) concentrations in the bulk electrolyte. In theory, these reactive oxygen species could be easily oxidized on the anode, which would yield a lower *FE* in the presence of O_2. Comparing the *FE* of the first run of experiments at *CDR* = 54 with and without aeration (O2_54, Lab_54) shows that the *FE* was slightly higher in the aerated system. This finding does not support the theory that reactive O_2 species have a considerable effect on the *FE*.

Fe-precipitate structure. Still, the presence or absence of oxygen might have an indirect effect on the *FE*. Its absence resulted in the formation of mixed valent iron oxide flocs (e.g. dark colored green rust) whereas small ferrihydrite like precipitates were formed in the presence of O_2 (Lab_04 & O2_54, compare Annex Figure 4). In the latter experiment, a higher surface layer mass was observed compared to the experiment without aeration at same *CDR,* suggesting a correlation between the type of Fe precipitate and the formation of larger SLs. The *FE* in this system was still high (> 0.8 after 15 runs), but a small decrease in *FE* was observed over time.

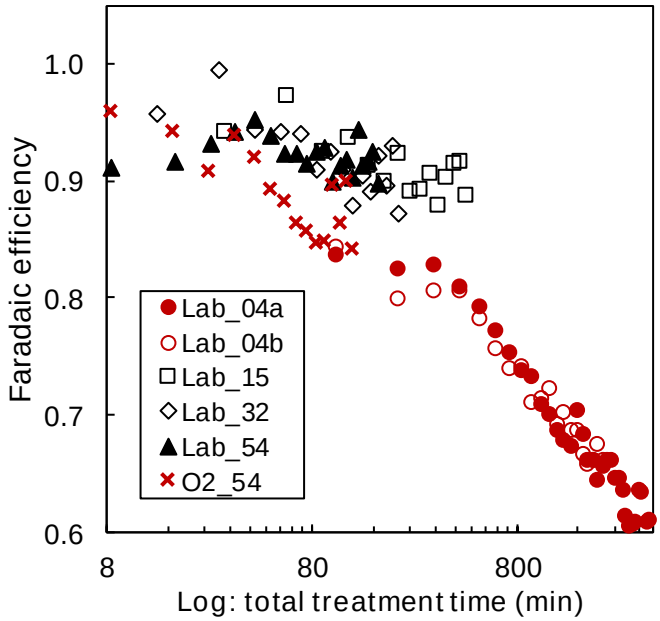

Figure 11. *FE* of experiments with laboratory steel anodes in SGW at different CDR vs the total electrolysis time (log axis). Experiments with consistent [O_2] > 3 mg/L shown in red.

Total electrolysis time. When the *CDR* is increased, but the total charge dose is maintained, the electrolysis time decreases. Instead of the number of runs, we plot the *FE* vs the total electrolysis time in Figure 11. The *FE* in the low-O_2 systems seems to be independent of electrolysis time, ranging from 8 – 30 min for *CDR*s of 54 – 15 C/L/min. In contrast, the *FE* of the oxic systems Lab_04 and O2_54 decreases over total electrolysis time. This effect is not linear, and the results suggest that the largest drop in *FE* occurs in the first 300 min.

Combined effects. The positive effect of elevated *CDR* on the *FE* is likely to be a combined effect of altered Fe-precipitate structure and different contact times: When small ferrihydrite like Fe(III)

precipitates are formed, longer contact time between precipitate and electrode surface results in larger SLs. This theory is consistent with the lower FE of 0.85 during the first run of Lab_04 with a treatment time of 105 min, similar to a total of 12 runs of O2_54. Yet, there is some scatter in the data from O2_54, the only oxic experiment performed at high *CDR*, and further investigation of the long-term trends is required.

4.2.2 Electrolyte composition

We observed a large effect of oxyanions (carbonate, silicate, and phosphate) on the *FE*, the presence of which in the electrolyte led to a lower initial *FE* and a decrease over time compared to electrolytes without oxyanions.

Passivation. A lower *FE* could be the result of anode passivation, which would increase the *IP* with the result of e.g. water oxidation instead of Fe(0) oxidation. A recent study observed *FEs* close to 0 in single-anion electrolytes containing either phosphate, carbonate, or nitrate (van Genuchten et al. 2017). The authors attributed these observations to oxyanions bonding to the oxidized Fe anode surface, which resulted in a passive layer that inhibited further Fe(0) oxidation. In our experiments, we observed an initial *FE* difference of about 0.1 between experiments in electrolytes with and without oxyanions. This difference is small compared to the reported passivation in Fe-EC system (*FE* ≈ 0). Nevertheless, the lower anodic interface potential when oxyanions were absent suggests that oxyanions in the electrolyte modified the anode surface.

Fe precipitate structure. Similar to the strong effect of *CDR* on the Fe precipitate structure and *FE*, we observed a correlation between the electrolyte composition and the Fe precipitates. When oxyanions where absent in the electrolyte, Fe oxides like lepidocrocite or magnetite were generated instead of small ferrihydrite-like precipitates. The decrease in *FE* over repeated operation and the formation of heavy anodic SLs was only observed in the presence of oxyanions, which suggests that oxyanions promote layer growth. One possible explanation is that oxyanions bind to surface sites during Fe(III) polymerization (van Genuchten et al. 2014)., which leads to small disordered precipitates. Smaller Fe precipitates might be more likely to be deposited compared to large flocs that settle quickly. Calcite formation on the cathode in the absence of oxyanions (Annex Figure 5, Oxyanion-free) did not decrease the long-term *FE,* which emphasizes the importance of oxyanions for layer formation and decreased efficiency.

Chloride effects. However, experiment NaCl_04 is an exception, because the heavier SL that was formed did not lead to a low *FE*. This feature might be related to pure NaCl electrolyte and the long treatment time of 105 min, possibly enhancing passive corrosion of the anode. Chloride is known to break down passive layers on iron (Pou et al. 1984), consistent with the observed low *IP,* and promotes the corrosion of steel (Cornell and Schwertmann 2003). Arroyo et al. (2009) investigated the effect of NaCl on the *FE* and found a FE > 1 at high Cl^- concentrations and low pH, which was attributed to increased Fe dissolution due to pitting corrosion. In comparison, the *FE* just below 1 in our NaCl experiments is possibly caused by the circumneutral pH which does not allow the

chemical dissolution of Fe(0). Similar to our results, van Genuchten et al. (2017) observed high *FE* ≈ 1 in NaCl electrolyte, independent of the *CDR*. Interestingly, their experiments in binary solutions of Cl^- and HCO_3^- or NO_3^- showed that high *FE* can still be achieved by the addition of sodium chloride. In our experiments, the high chloride concentrations (≥ 8 mM) in all electrolytes could explain why complete anode passivation did not occur despite the high oxyanion concentrations (8 mM HCO_3^-, 1 mM SiO_3^{2-}) in the SGW electrolyte.

4.3 Implications for field EC systems

4.3.1 Maintaining high *FE*

For As removal with Fe-EC, it is crucial that two main processes occur: First, the applied current oxidizes Fe(0) to Fe(II) and the dissolved Fe migrates to the bulk electrolyte. Second, Fe(II) is oxidized by dissolved O_2 which produces reactive intermediates (responsible for As(III) oxidation) and solid Fe precipitates that bind As (van Genuchten et al. 2016). The first step was investigated in this study by quantifying the amount of Fe in the bulk electrolyte under varying conditions. We discussed the key parameters observed to impact Fe production in EC over extended operation. The implications for real EC-systems and possible implications for As removal will be addressed in the following section.

The purity of the anode material had no significant effect on the long-term *FE*, which is especially positive for the application of EC systems in remote areas. The use of locally available steel of unknown purity makes it easier to implement Fe-EC as treatment technology on a larger scale. However, both the anode interface potential and cell voltage showed a stronger increase when impure anodes were used, so a steel of higher purity should be favored if available at reasonable costs.

In our experiments, the most significant result was the strong impact of the *CDR* on the *FE*, because the current can be adjusted easily with existing infrastructure. We found that a *CDR* of 15 C/L/min (equivalent to a current density of 2.8 mA/cm^2 in our system) led to a higher and more stable *FE* compared to a *CDR* of 4 C/L/min. A high *FE,* but especially a stable iron generation over time is key for an efficient and reliable treatment system. A negative effect of higher *CDR* was the higher electric energy consumption (see section 4.3.2). Positive, especially in areas with intermittent electricity supply, is the shorter treatment time achieved. Increasing the *CDR* further (> 15 C/L/min) had no effect on the *FE* and is only recommended if shorter treatment time are required.
In addition, at *CDR* ≥ 15 C/L/min, the oxygen concentrations dropped and different iron precipitates, likely green rusts, were formed in our system. While green rust can also bind arsenic (Wang et al. 2010), the low oxygen concentrations are likely to have a negative effect on the removal of As(III) (Delaire et al. 2017). These effects should be evaluated for the specific Fe-EC reactor before higher *CDR* are applied to remove arsenic.

We also found that electrolyte composition was a key parameter for the *FE*. However, modifying the electrolyte composition is not practical prior to treatment, in fact, the removal of oxyanions (like As) or other constituents is the aim of Fe-EC. The addition of Cl^- could improve the performance of Fe-EC in electrolytes rich in oxyanions, but may have negative effects on the acceptability of (treated) drinking water. The WHO recommends to avoid Cl^- concentrations above 250 mg/L (≈ 7 mmol/L), which is approximately the taste threshold for NaCl, but there is no health related guideline for drinking water (WHO 2017). In our study, Cl^- concentrations did already exceed 7 mmol/L, so further NaCl addition seems not an appropriate measure, but could be an option for water sources high in oxyanions (phosphate, carbonate, nitrate, ...) and low in chloride.

Mechanical cleaning of electrodes, the complete removal of the surface layers, is another option to increase the FE and decrease the cell voltage, but does not prevent subsequent surface layer formation and decreasing *FE*. It is recommended when other options are not applicable to avoid FE below a threshold, but it requires a large workforce. Acid treatment, although very effective, introduce disposal problems and requires skilled labor. Our preliminary experiments with mild acids (lemon juice) cannot be used to give recommendations yet.

Alternating the polarity, which is also performed in the field system, did have a negative effect on the *FE* in our experiments. When the polarity was only switched between experiments, the negative effect on the *FE* was smaller, but a low and stable cell voltage over time was achieved. In addition, the structure of the surface layers changed due to the precipitation of calcite on both electrodes which might facilitate the mechanical removal of these layers. In consequence, the polarity switch should be maintained, but shorter cycles are not recommended based on our results.

4.3.2 Electric energy consumption

In addition to a high and stable *FE*, a low electricity consumption per treated volume is desired to achieve cost-efficient treatment. We applied a constant current and the corresponding cell voltage was measured after one fifth electrolysis time and at the end of electrolysis. In most experiments, the highest voltage was measured at the start of the experiment, which is reported in Table 4.
The cell voltage depends mainly on the distance between the electrodes (1 cm in all experiments), the electrolyte conductivity (see Table 2), the current density (which was set, Table 3) and properties of the electrode surface, including submerged surface area and presence of an insulating SL (Chen et al. 2002). Consequently, the average cell voltage increased when higher currents were applied, because the overpotential increases with the applied current density (e.g. Lab_04, Lab_15, Lab_32, etc.) (Chen et al. 2002). Although a higher current resulted in a shorter treatment time – we maintained a total dose of 450 C/L in all experiments – it still increased electricity consumption.

In general, the cell voltage increased with the number of runs and we attribute this to the changes at the electrode surface, as all other key parameters remained constant. There were only three experiments that showed no increase in cell voltage over time: the experiments with alternating polarity and electrode storage in water. That is surprising given the low *FE* and heavy SL in these

systems, but consistent with literature that recommends polarity reversal to prevent passive layers (Hansen et al. 2007, Vasudevan et al. 2011, Yang et al. 2015).
The field anode material, which had no significant effect on the long-term *FE*, showed a larger increase in cell voltage over the first 15 runs compared to the lab anode. This effect was strongest at high *CDR* and the voltage increased by 4 V (Field_54) compared to only 1 V (Lab_54), which is a disadvantage for the overall treatment efficiency. Polarity reversal experiments with the field anode material might overcome such problems, but could not be tested due to limited amount of field anode.

Table 4. Average Faradaic efficiency (*FE*), average cell voltage measured after 1/5th of electrolysis time (U_{cell}), and average electric energy consumption (EEC) for electrolysis for the first 15 runs of each experiment. The change in cell voltage over 15 runs ΔU_{cell} indicates the long-term trend (calculated from average U_{cell} of run 1 – 3 and run 13 – 15).

Experiment	*FE* average	SD	EEC average kWh/m^3	U_{cell} average V	SD	**ΔU_{cell}** 15 runs V
Lab_04a	0.75	± 0.06	0.26	2.06	± 0.05	+ 0.05
Lab_04b	0.75	± 0.05	0.26	2.07	± 0.05	+ 0.07
Field_04	0.70	± 0.07	0.20	1.63	± 0.17	+ 0.37
Lab_15	0.91	± 0.02	0.49	3.94	± 0.36	+ 0.80
Lab_32	0.92	± 0.03	0.86	6.86	± 0.77	+ 1.84
Lab_54	0.92	± 0.01	1.17	9.31	± 0.42	+ 1.04
Field_54	0.90	± 0.04	1.13	8.83	± 1.63	+ 4.01
O2_54	0.89	± 0.04	1.35	10.76	± 1.15	+ 2.85
Soft-SGW	0.75	± 0.05	0.22	1.83	± 0.06	+ 0.09
Oxyanion-free	0.94	± 0.03	0.27	2.10	± 0.15	+ 0.37
NaCl_04	0.93	± 0.03	0.23	1.80	± 0.06	+ 0.09
NaCl_54	0.94	± 0.02	1.48	11.85	± 0.20	+ 0.10
Polarity-1	0.72	± 0.09	0.21	1.62	± 0.27	- 0.60
Polarity-5	0.60	± 0.09	0.22	1.81	± 0.10	- 0.21
SGW-storage	0.63	± 0.10	0.24	1.86	± 0.14	- 0.15

4.4 Future work

Based on the results of our work, several new research questions were raised while some remained unanswered. We found a *CDR* of 15 C/L/min had a positive effect on the *FE*, but increasing the *CDR* further increased only the electricity consumption. Future research could identify the ideal *CDR* to achieve a high and stable *FE* at low electricity consumption, most likely between 4 and 15 C/L/min. The effect of higher *CDR* on arsenic removal should be evaluated.

We found indications that the higher *FE* at higher *CDR* are the result of low O_2 conditions and/or different Fe precipitates, but no clear long-term trend when high O_2 concentrations were maintained at high *CDR*. Experiments at elevated *CDR* at different oxygen concentrations would add important

information. In addition, experiments to investigate current density and *CDR* separately would be useful, as the anode surface area to volume ratio was the same in all our experiments.

While polarity reversal had a negative effect on the *FE* and SL formation, it also decreased electricity consumption. We investigated the effect of polarity reversal only at low *CDR*. Alternating the polarity at elevated *CDR* could be a promising technique to limit layer formation at lower electricity consumption and should be investigated in more detail.

5. Conclusions

The aim of this study was to investigate if long-term operation leads to a decrease in *FE*, a potential reason for a lower arsenic removal efficiency of field EC-systems. Our results showed that the *FE* continuously decreased over time and reached a *FE* of 0.6 after 35 runs, when operating conditions similar to a system used for arsenic removal in West Bengal were applied. The accordingly lower iron dose can result in a lower arsenic removal efficiency and needs to be considered in the operation of Fe-EC systems.

Our experiments under various conditions showed that the lower long-term *FE* was not caused by a low Fe(0) anode purity. Instead, the electrolyte composition and the charge dosage rate *(CDR)* were identified as key parameters governing the *FE*. Applying a *CDR* ≥ 15 C/L/min or excluding oxyanions from the electrolyte affected Fe precipitate formation and correlated with surface layers of lower mass on the anode surface. Consequently, the loss of iron from the bulk electrolyte by deposition on the electrodes (surface layer formation) rather than competing anode reactions (due to passivation) was likely the main cause for the decreasing *FE* under field conditions.

Hence, a high and stable *FE* in field systems can be achieved by increasing the applied current (*CDR*) or by complete removal of the surface layer. The side effects of higher *CDR*, a lower O_2 concentration in the electrolyte and altered Fe precipitates, require further investigation with respect to the effect on arsenic removal.

Annex

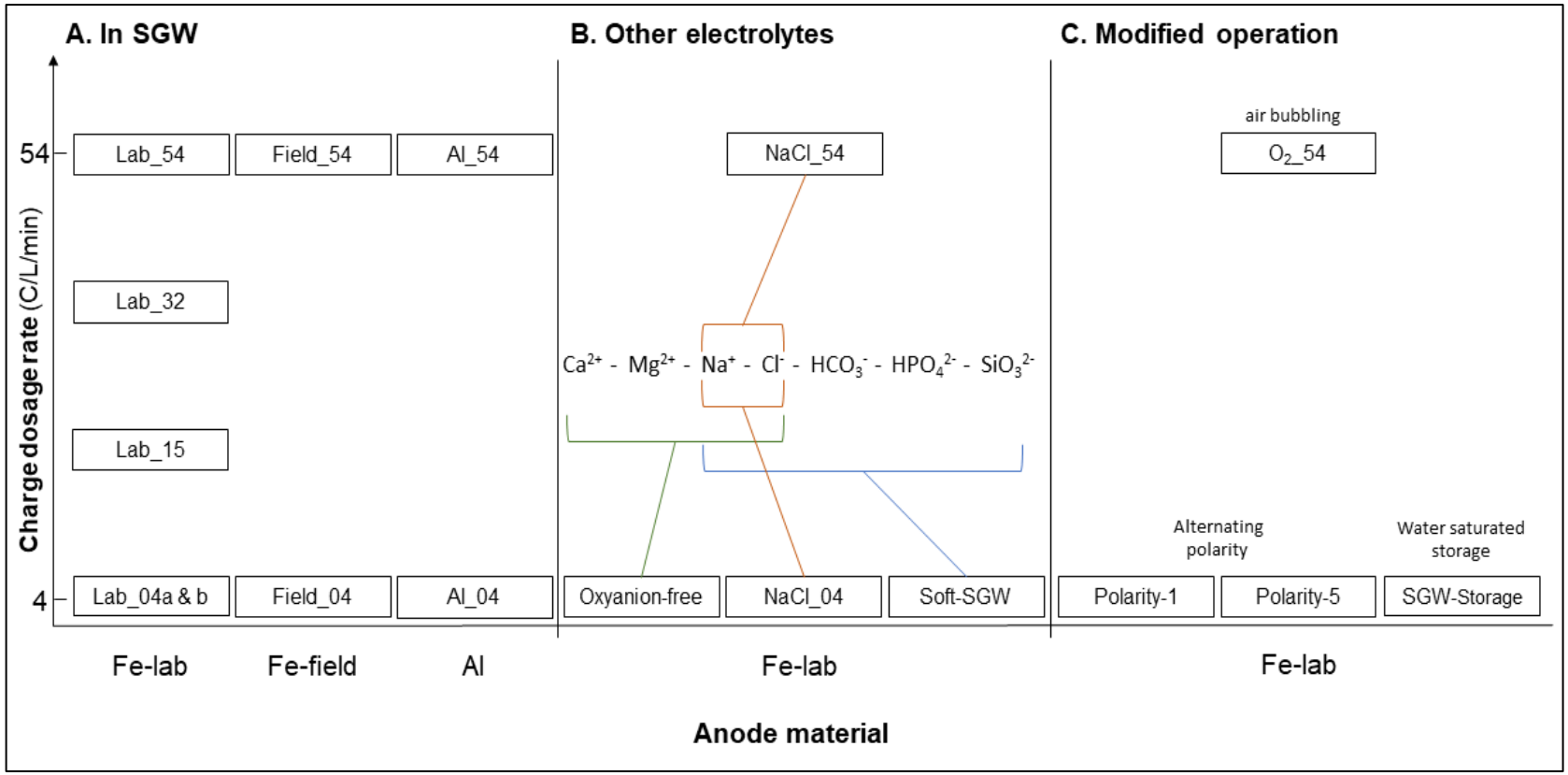

Annex Figure 1. Overview of all experiments separated by charge dosage rate and Anode material. **A.** Experiments with different anode materials in SGW. **B.** Experiments with Fe-anodes in different electrolytes. **C.** Modified operation and storage with Fe-anodes in SGW.

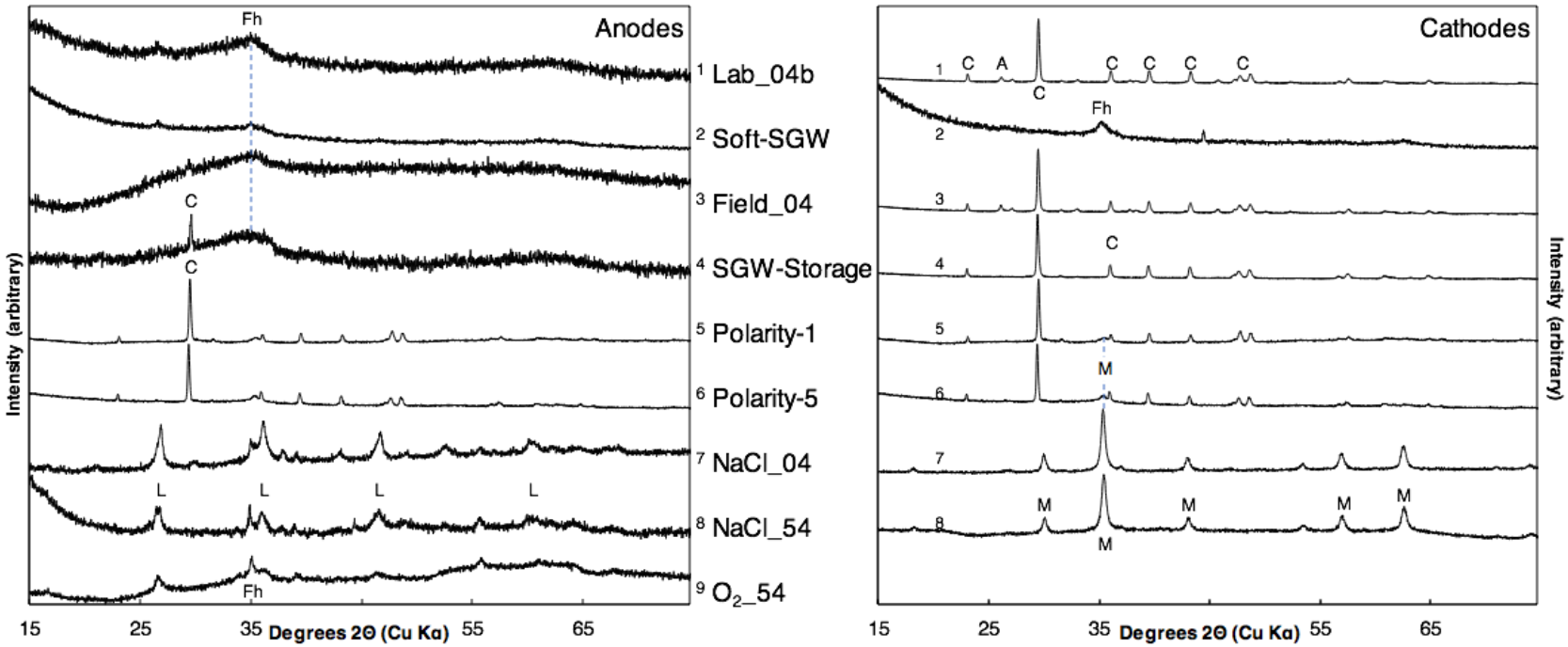

Annex Figure 2. Powder XRD patterns of layer samples brushed from the surface of representative experiments. Peaks due to the presence of lepidocrocite (L), magnetite (M), calcite (C), and aragonite (A) are indicated. Broader peaks at 35° indicate the presence of a poorly crystalline Fe phase similar to ferrihydrite (Fh).

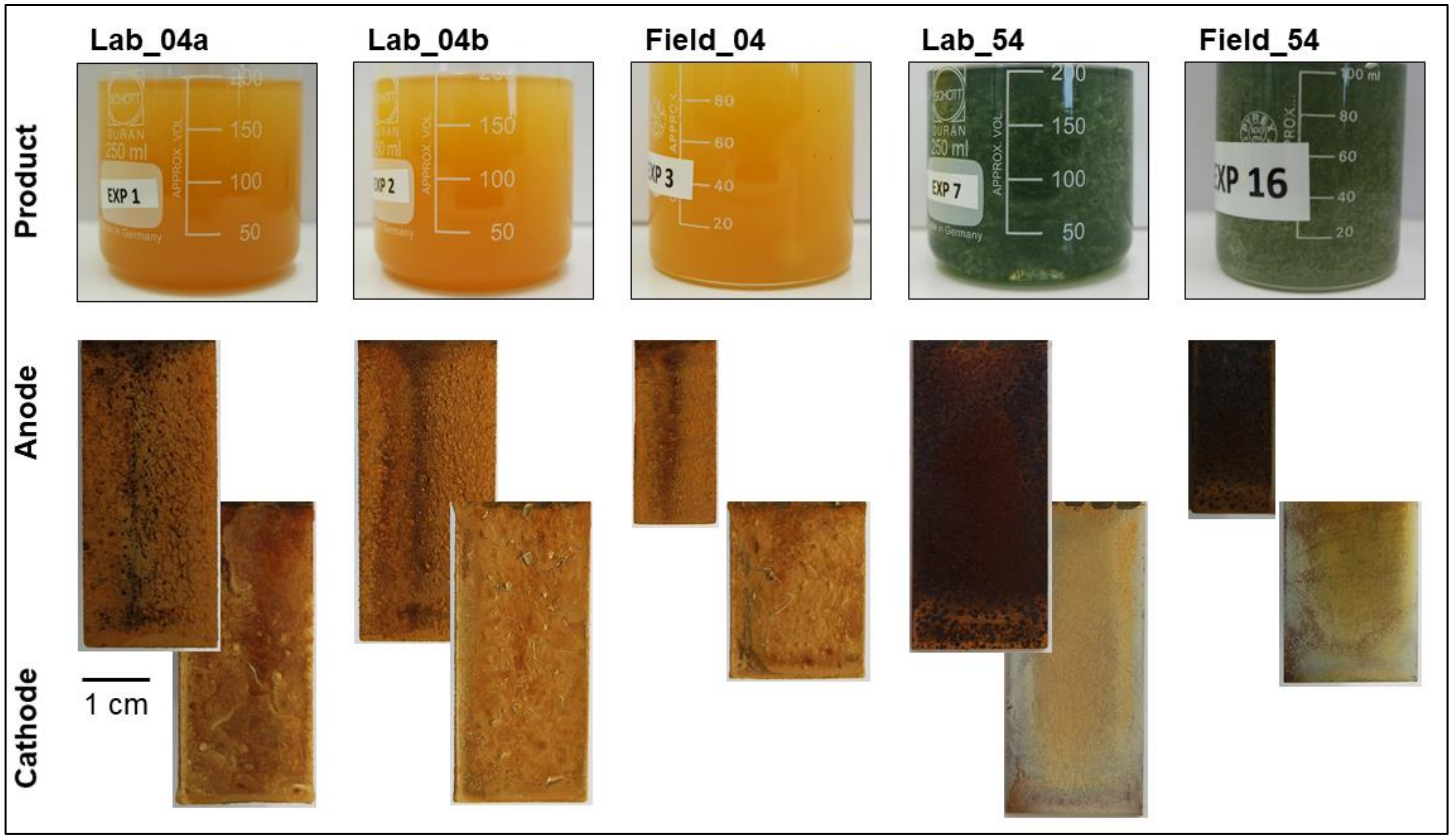

Annex Figure 3. Product and surface layer of laboratory electrodes and field anode at low and high *CDR*.

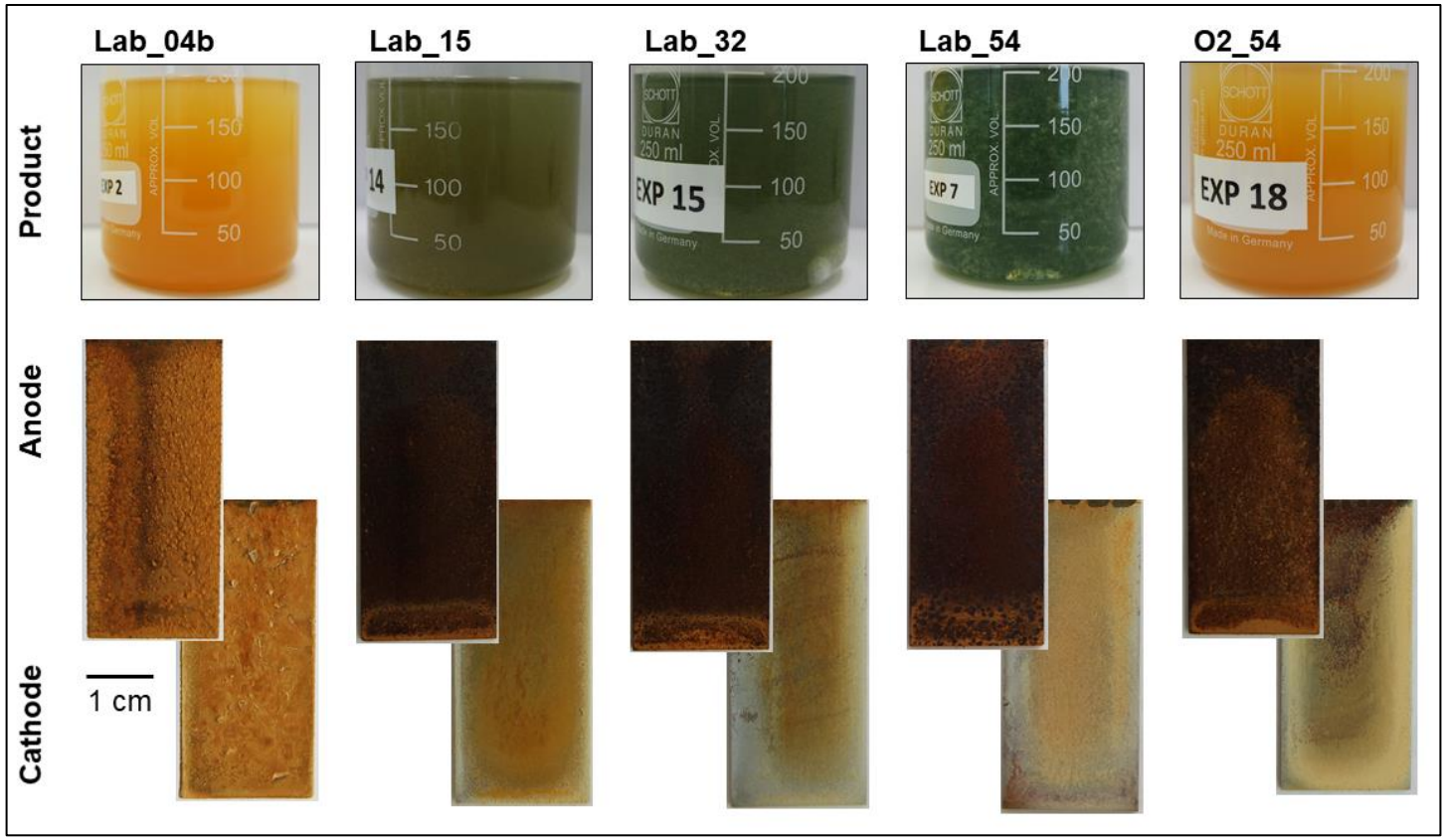

Annex Figure 4. Product and surface layer at different *CDR*.

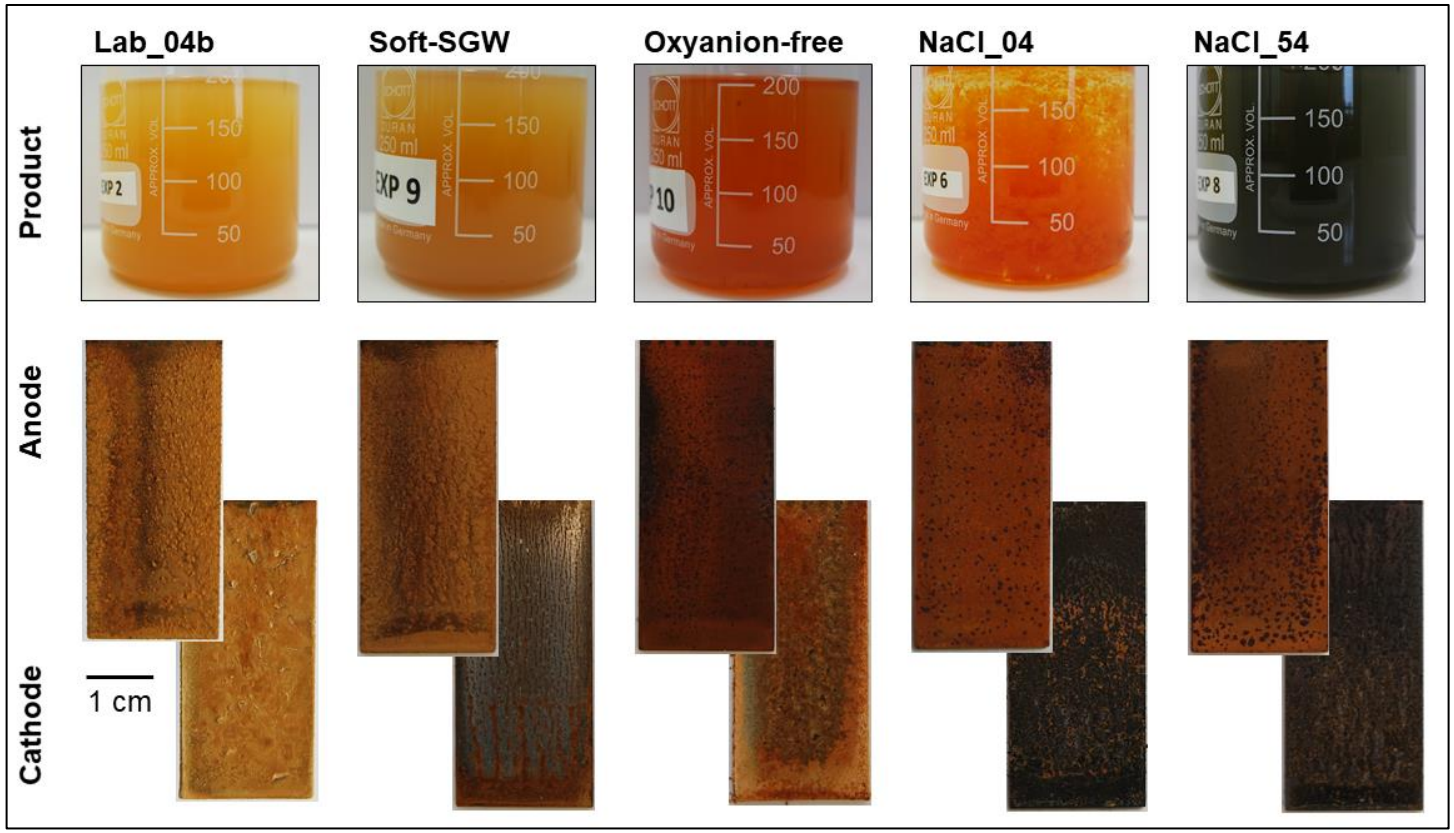

Annex Figure 5. Product and surface layer for different electrolyte compositions.

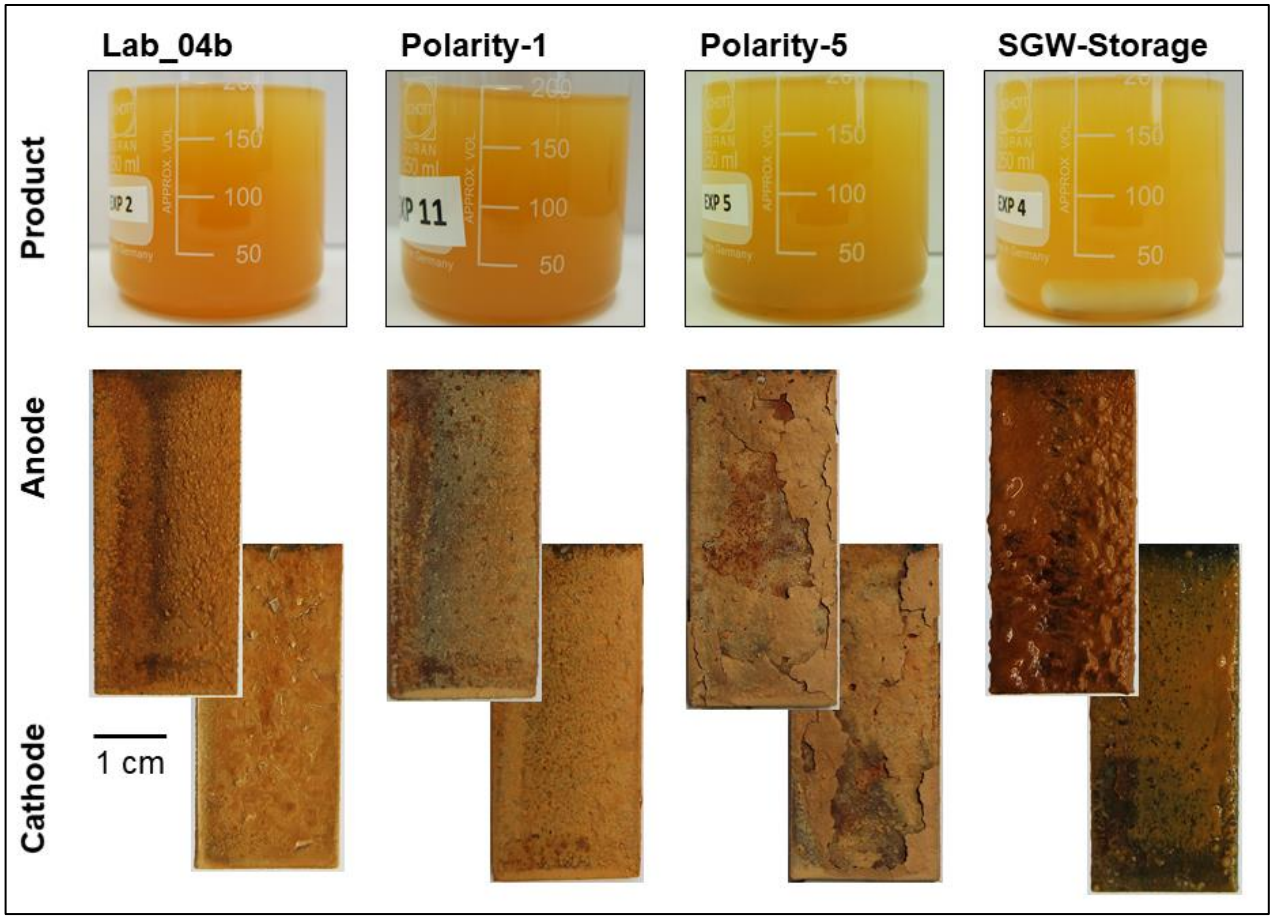

Annex Figure 6. Product and surface layer for different operation and storage modifications at low *CDR* in SGW.

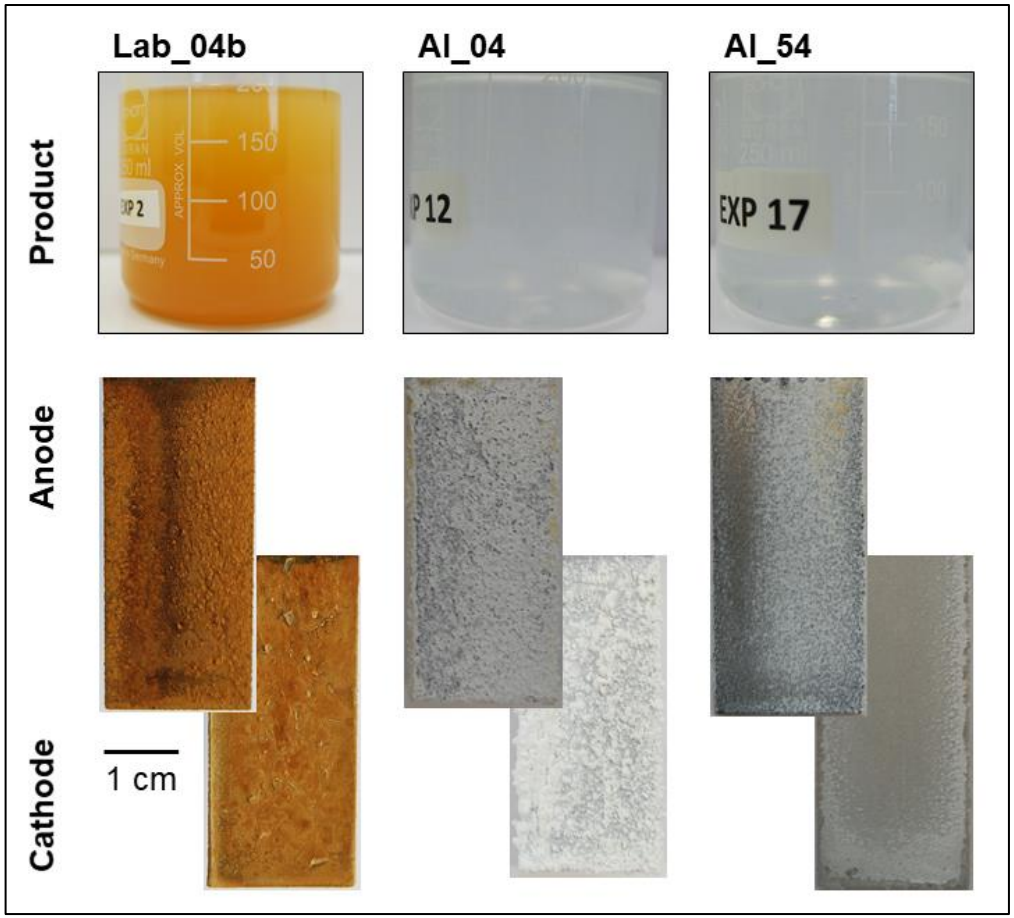

Annex Figure 7. Product and surface layer of Al electrodes compared to Fe electrodes.

References

Akbal, F. and Camcı, S. (2011) Copper, chromium and nickel removal from metal plating wastewater by electrocoagulation. Desalination 269(1), 214-222.

Aleboyeh, A., Daneshvar, N. and Kasiri, M. (2008) Optimization of CI Acid Red 14 azo dye removal by electrocoagulation batch process with response surface methodology. Chemical Engineering and Processing: Process Intensification 47(5), 827-832.

Amrose, S.E., Bandaru, S.R., Delaire, C., van Genuchten, C.M., Dutta, A., DebSarkar, A., Orr, C., Roy, J., Das, A. and Gadgil, A.J. (2014) Electro-chemical arsenic remediation: field trials in West Bengal. Sci Total Environ 488-489, 539-546.

APHA (2005) Standard Methods for the Examination of Water & Wastewater, American Public Health Association (APHA), Washington, DC, USA.

Argos, M., Kalra, T., Rathouz, P.J., Chen, Y., Pierce, B., Parvez, F., Islam, T., Ahmed, A., Rakibuz-Zaman, M., Hasan, R., Sarwar, G., Slavkovich, V., van Geen, A., Graziano, J. and Ahsan, H. (2010) Arsenic exposure from drinking water, and all-cause and chronic-disease mortalities in Bangladesh (HEALS): a prospective cohort study. The Lancet 376(9737), 252-258.

Arroyo, M., Pérez-Herranz, V., Montanes, M., Garcia-Anton, J. and Guinon, J. (2009) Effect of pH and chloride concentration on the removal of hexavalent chromium in a batch electrocoagulation reactor. Journal of hazardous materials 169(1), 1127-1133.

Bard, A.J. and Faulkner, L.R. (2001) Electrochemical Methods: Fundamentals and Applications, John Wiley & Sons.

BGS and DPHE (2001) Arsenic contamination of groundwater in Bangladesh. Kinniburgh, D.G. and Smedley, P.L. (eds), British Geological Survey, Keyworth.

Chen, X., Chen, G. and Yue, P.L. (2000) Separation of pollutants from restaurant wastewater by electrocoagulation. Separation and Purification Technology 19(1), 65-76.

Chen, X., Chen, G. and Yue, P.L. (2002) Investigation on the electrolysis voltage of electrocoagulation. Chemical Engineering Science 57(13), 2449-2455.

Cornell, R.M. and Schwertmann, U. (2003) The iron oxides: structure, properties, reactions, occurrences and uses, John Wiley & Sons.

Delaire, C., Amrose, S., Zhang, M., Hake, J. and Gadgil, A. (2017) How do operating conditions affect As(III) removal by iron electrocoagulation? Water Res 112, 185-194.

Delaire, C., van Genuchten, C.M., Nelson, K.L., Amrose, S.E. and Gadgil, A.J. (2015) Escherichia coli attenuation by Fe electrocoagulation in synthetic Bengal groundwater: effect of pH and natural organic matter. Environmental Science & Technology 49(16), 9945-9953.

Dubrawski, K.L., van Genuchten, C.M., Delaire, C., Amrose, S.E., Gadgil, A.J. and Mohseni, M. (2015) Production and transformation of mixed-valent nanoparticles generated by Fe(0) electrocoagulation. Environ Sci Technol 49(4), 2171-2179.

Flanagan, S.V., Johnston, R.B. and Zheng, Y. (2012) Arsenic in tube well water in Bangladesh: health and economic impacts and implications for arsenic mitigation. Bulletin of the World Health Organization 90(11), 839-846.

Frankel, G. (1998) Pitting corrosion of metals a review of the critical factors. Journal of the Electrochemical Society 145(6), 2186-2198.

Hansen, H.K., Nunez, P., Raboy, D., Schippacasse, I. and Grandon, R. (2007) Electrocoagulation in wastewater containing arsenic: Comparing different process designs. Electrochimica Acta 52(10), 3464-3470.

Hering, J.G., Chen, P.-Y., Wilkie, J.A. and Elimelech, M. (1997) Arsenic removal from drinking water during coagulation. Journal of Environmental Engineering 123(8), 800-807.

Hug, S.J. and Leupin, O. (2003) Iron-Catalyzed Oxidation of Arsenic(III) by Oxygen and by Hydrogen Peroxide: pH-Dependent Formation of Oxidants in the Fenton Reaction. Environmental Science & Technology 37(12), 2734-2742.

Kelly, R.G., Scully, J.R., Shoesmith, D. and Buchheit, R.G. (2002) Electrochemical techniques in corrosion science and engineering, CRC Press.

Lakshmanan, D., Clifford, D.A. and Samanta, G. (2009) Ferrous and Ferric Ion Generation During Iron Electrocoagulation. Environ. Sci. Technol. 43(10), 3853-3859.

Li, L., van Genuchten, C.M., Addy, S.E., Yao, J., Gao, N. and Gadgil, A.J. (2012) Modeling As(III) oxidation and removal with iron electrocoagulation in groundwater. Environ Sci Technol 46(21), 12038-12045.

Lokuge, K.M., Smith, W., Caldwell, B., Dear, K. and Milton, A.H. (2004) The effect of arsenic mitigation interventions on disease burden in Bangladesh. Environmental Health Perspectives 112(11), 1172.

Mansoorian, H.J., Mahvi, A.H. and Jafari, A.J. (2014) Removal of lead and zinc from battery industry wastewater using electrocoagulation process: influence of direct and alternating current by using iron and stainless steel rod electrodes. Separation and Purification Technology 135, 165-175.

Mansouri, K., Elsaid, K., Bedoui, A., Bensalah, N. and Abdel-Wahab, A. (2011) Application of electrochemically dissolved iron in the removal of tannic acid from water. Chemical Engineering Journal 172(2), 970-976.

Mechelhoff, M., Kelsall, G.H. and Graham, N.J.D. (2013) Super-faradaic charge yields for aluminium dissolution in neutral aqueous solutions. Chemical Engineering Science 95, 353-359.

Mohan, D. and Pittman, C.U. (2007) Arsenic removal from water/wastewater using adsorbents—A critical review. Journal of hazardous materials 142(1), 1-53.

Mollah, M.Y., Morkovsky, P., Gomes, J.A., Kesmez, M., Parga, J. and Cocke, D.L. (2004) Fundamentals, present and future perspectives of electrocoagulation. Journal of hazardous materials 114(1), 199-210.

Mollah, M.Y.A., Schennach, R., Parga, J.R. and Cocke, D.L. (2001) Electrocoagulation (EC)—science and applications. Journal of hazardous materials 84(1), 29-41.

Nickson, R., McArthur, J., Burgess, W., Ahmed, K.M., Ravenscroft, P. and Rahmann, M. (1998) Arsenic poisoning of Bangladesh groundwater. Nature 395(6700), 338.

Nordstrom, D.K. (2002) Worldwide occurrences of arsenic in ground water. Science 296(5576), 2143-2145.

Pallier, V., Feuillade-Cathalifaud, G. and Serpaud, B. (2011) Influence of organic matter on arsenic removal by continuous flow electrocoagulation treatment of weakly mineralized waters. Chemosphere 83(1), 21-28.

Pan, C., Troyer, L.D., Catalano, J.G. and Giammar, D.E. (2016) Dynamics of chromium (VI) removal from drinking water by iron electrocoagulation. Environmental Science & Technology 50(24), 13502-13510.

Pou, T.E., Murphy, O.J., Young, V., Bockris, J.O.M. and Tongson, L.L. (1984) Passive films on iron: the mechanism of breakdown in chloride containing solutions. Journal of the Electrochemical Society 131(6), 1243-1251.

Roberts, L.C., Hug, S.J., Ruettimann, T., Billah, M.M., Khan, A.W. and Rahman, M.T. (2004) Arsenic Removal with Iron(II) and Iron(III) in Waters with High Silicate and Phosphate Concentrations. Environmental Science & Technology 38(1), 307-315.

Schultze, J.W. and Lohrengel, M. (2000) Stability, reactivity and breakdown of passive films. Problems of recent and future research. Electrochimica Acta 45(15), 2499-2513.

Schwertmann, U. and Cornell, R.M. (2000) Iron oxides in the laboratory: preparation and characterization, John Wiley & Sons.

Sharma, A.K., Tjell, J.C., Sloth, J.J. and Holm, P.E. (2014) Review of arsenic contamination, exposure through water and food and low cost mitigation options for rural areas. Applied Geochemistry 41, 11-33.

Sillanpää, M. and Shestakova, M. (2017) Electrochemical Water Treatment Methods: Fundamentals, Methods and Full Scale Applications, Butterworth-Heinemann.

Timmes, T.C., Kim, H.-C. and Dempsey, B.A. (2009) Electrocoagulation pretreatment of seawater prior to ultrafiltration: Bench-scale applications for military water purification systems. Desalination 249(3), 895-901.

Timmes, T.C., Kim, H.-C. and Dempsey, B.A. (2010) Electrocoagulation pretreatment of seawater prior to ultrafiltration: Pilot-scale applications for military water purification systems. Desalination 250(1), 6-13.

van Genuchten, C.M., Addy, S.E., Pena, J. and Gadgil, A.J. (2012) Removing arsenic from synthetic groundwater with iron electrocoagulation: an Fe and As K-edge EXAFS study. Environ Sci Technol 46(2), 986-994.

van Genuchten, C.M., Bandaru, S.R., Surorova, E., Amrose, S.E., Gadgil, A.J. and Pena, J. (2016) Formation of macroscopic surface layers on Fe(0) electrocoagulation electrodes during an extended field trial of arsenic treatment. Chemosphere 153, 270-279.

van Genuchten, C.M., Dalby, K.N., Ceccato, M., Stipp, S.L.S. and Dideriksen, K. (2017) Factors affecting the Faradaic efficiency of Fe(0) electrocoagulation. submitted to the Journal of Environmental Chemical Engineering.

van Genuchten, C.M., Peña, J., Amrose, S.E. and Gadgil, A.J. (2014) Structure of Fe (III) precipitates generated by the electrolytic dissolution of Fe (0) in the presence of groundwater ions. Geochimica et Cosmochimica Acta 127, 285-304.

Vasudevan, S., Kannan, B.S., Lakshmi, J., Mohanraj, S. and Sozhan, G. (2011) Effects of alternating and direct current in electrocoagulation process on the removal of fluoride from water. Journal of Chemical Technology and Biotechnology 86(3), 428-436.

Wang, Y., Morin, G., Ona-Nguema, G., Juillot, F., Guyot, F., Calas, G. and Brown, G.E. (2010) Evidence for Different Surface Speciation of Arsenite and Arsenate on Green Rust: An EXAFS and XANES Study. Environmental Science & Technology 44(1), 109-115.

WHO (2017) Guidelines for drinking-water quality: fourth edition incorporating the first addendum., World Health Organization, Geneva.

Xie, S., Yuan, S., Liao, P., Tong, M., Gan, Y. and Wang, Y. (2017) Iron-anode enhanced sand filter for arsenic removal from tube well water. Environmental Science & Technology 51(2), 889-896.

Yang, Z.-h., Xu, H.-y., Zeng, G.-m., Luo, Y.-l., Yang, X., Huang, J., Wang, L.-k. and Song, P.-p. (2015) The behavior of dissolution/passivation and the transformation of passive films during electrocoagulation: influences of initial pH, Cr (VI) concentration, and alternating pulsed current. Electrochimica Acta 153, 149-158.